2010

A multi-instrument study of auroral hiss at Saturn

Andrew James Kopf
University of Iowa

A MULTI-INSTRUMENT STUDY OF AURORAL HISS AT SATURN

by

Andrew James Kopf

An Abstract

Of a thesis submitted in partial fulfillment
of the requirements for the
Doctor of Philosophy degree in Physics
in the Graduate College of
The University of Iowa

July 2010

Thesis Supervisor: Professor Donald A. Gurnett

ABSTRACT

Over the last fifty years, a multitude of spacecraft and rocket experiments have studied plasma wave emissions from Earth's auroral regions. One such emission is auroral hiss, a low-frequency whistler-mode wave that is produced in the auroral zone. Observations from Earth-orbiting spacecraft show that auroral hiss is generated by field-aligned electron beams, with the resulting plasma wave emission propagating along the resonance cone. This propagation results in auroral hiss appearing as a V-shaped funnel when observed on a frequency-time spectrogram. This thesis presents the first comprehensive study of auroral hiss at a planet other than Earth, using the Cassini spacecraft to study auroral hiss at Saturn.

NASA's Cassini spacecraft, currently in orbit around Saturn, has allowed for the first opportunity to study this emission in detail at another planet. Since 2006, the Cassini spacecraft has twice been in a series of high inclination orbits, allowing investigation and measurements of Saturnian auroral phenomena. During this time, the Radio and Plasma Wave Science (RPWS) Investigation on Cassini detected low frequency whistler mode emissions propagating upward along the auroral field lines, much like terrestrial auroral hiss. Comparisons of RPWS data with observations from several other Cassini instruments, including the Dual-Technique Magnetometer (MAG), Magnetospheric Imaging Instrument (MIMI), and the Cassini Plasma Spectrometer (CAPS), have revealed a complete picture of this emission at Saturn.

Observations from these instruments have been used to make a variety of determinations about auroral hiss at Saturn. RPWS has only observed this emission when Cassini was at high-latitudes, although these observations have shown no preference for local time. Tracking the times this emission has been observed revealed a clear periodicity in the emission. Further study

later revealed not one but two rotational modulations, one in each hemisphere, rotating at rates of 813.9 and 800.7 degrees per day in the northern and southern hemispheres, respectively. These rates match with observations of the clock-like Saturn Kilometric Radiation. Study of the field-aligned current structures in the auroral regions revealed a strong upward-directed current in both hemispheres on the lower-latitude side of the auroral hiss emission. Along with correlating particle densities, these observations were used to infer the presence of a high-density plasmasphere at low latitudes, with the series of field-aligned current structures lining up with the outer boundary at L-shell values of around 12-15.

Analysis of electron beams observed in conjunction with auroral hiss shows that these beams produce large growth rates for whistler-mode waves propagating along the resonance cone, similar to terrestrial auroral hiss. Analytical calculation of the normalized growth rates of ten electron beam events on Day 291, 2008, yielded a wide range of growth rates, from 0.004 to over 6.85 times the real frequency. The latter, a non-physical result, came from a violation of the weak growth approximation, suggesting there was so much growth that the analytical calculation was not valid in this instance. Numerical calculation using a plasma dispersion-solving code called WHAMP produced a growth rate of about 0.3, a still very large number, suggesting the detected beams may be the source of the observed auroral hiss plasma wave emission.

Abstract Approved:

_____

Thesis Supervisor

_____

Title and Department

_____

Date

A MULTI-INSTRUMENT STUDY OF AURORAL HISS AT SATURN

by

Andrew James Kopf

A thesis submitted in partial fulfillment
of the requirements for the
Doctor of Philosophy degree in Physics
in the Graduate College of
The University of Iowa

July 2010

Thesis Supervisor: Professor Donald A. Gurnett

Graduate College
The University of Iowa
Iowa City, Iowa

CERTIFICATE OF APPROVAL

_____

PH.D. THESIS

_____

This is to certify that the Ph.D. thesis of

Andrew James Kopf

has been approved by the Examining Committee for the thesis requirement for the Doctor of Philosophy degree in Physics at the July 2010 graduation.

Thesis Committee: _____
Donald Gurnett, Thesis Supervisor

_____
Robert Mutel

_____
Robert Merlino

_____
Gregory Howes

_____
Robert Yager

TABLE OF CONTENTS

LIST OF FIGURES

CHAPTER 1

INTRODUCTION

Auroral hiss is a plasma wave emission which frequently occurs in high-latitude regions of planetary magnetospheres. This emission was first discovered using ground based instruments [*Martin et al.*, 1960], which detected a very low frequency broadband emission in association with aurora. The first satellite observations of auroral hiss were made at the Earth in the 1960s [e.g. *Gurnett and O'Brien,* 1964*; Gurnett*, 1966; *McEwen and Barrington*, 1967; *Laaspere et al.,* 1971], and similar emissions have since been detected at other planets in the solar system, including Jupiter [*Gurnett et al.,* 1979; *Farrell et al.*, 1993; *Gurnett et al.,* 2005a] and Saturn [*Xin et al.*, 2006b; *Gurnett et al.*, 2009b]. Auroral hiss is known to propagate in the whistler mode, as the frequency is always above the local proton cyclotron frequency and below both the electron cyclotron frequency and electron plasma frequency. Whistler mode waves are the only plasma waves that can propagate in this range of frequencies. On a frequency-time spectrogram, this emission displays a characteristic funnel shape with a V-shaped low-frequency cutoff, as shown by *Gurnett* [1966]. The emission's V-shaped nature is explained by emission from a localized source propagating near the resonance cone [*Smith*, 1969; *Mosier and Gurnett*, 1969; *James*, 1976].

The resonance cone is defined as a cone of angles with respect to the magnetic field where the index of refraction goes to infinity, and denotes the region around the magnetic field line in which the emission is restricted to propagate. The resonance cone also imposes a restriction on the group velocity, the propagation of wave energy, to a region of angles around the field line. This boundary is a property of the index of refraction, $n(\theta)$, where θ is the angle the propagation vector (also known as the k-vector) makes with the central field line. This is

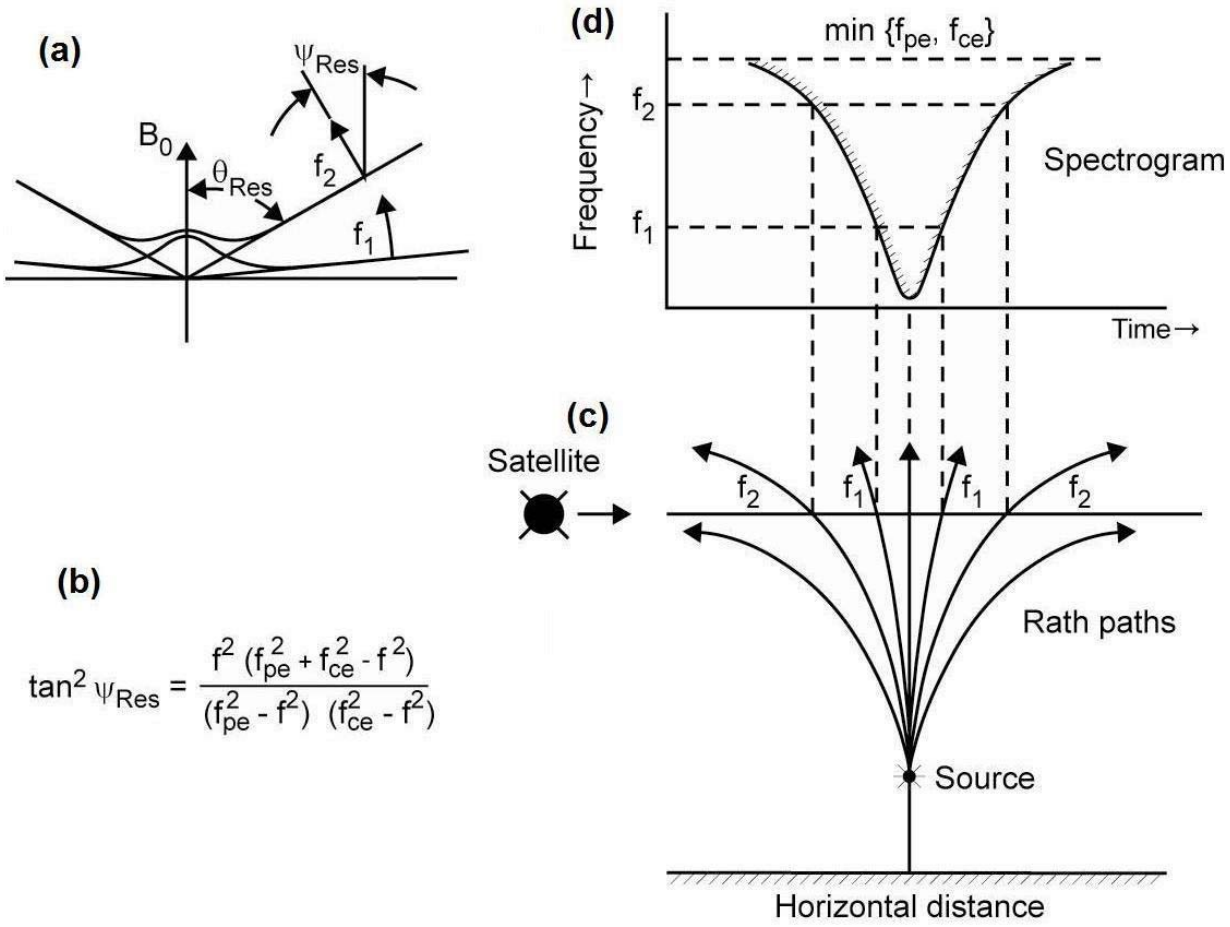

Figure 1 – Propagation of auroral hiss emission along the resonance cone. Sections (a) and (b) display geometrically and mathematically the computation of the resonance cone angle, while sections (c) and (d) describe the frequency-dependent propagation and explain its effect on how the data appear on a spectrogram.

shown in Figure 1(a). As the k-vector deviates further from the magnetic field direction, it approaches an angle where the index of refraction asymptotes to infinity [*Gurnett and Bhattacharjee*, 2005]. This angle is defined as θ_{res}. From this angle, we can define the limiting group velocity angle, ψ_{res}, which can be shown to always be perpendicular to the index of refraction surface, which along the resonance cone is given by $\psi_{res} = 90 - \theta_{res}$, in units of degrees.

This condition, however, is not uniform for all components of the emission. As shown by the equation in Figure 1(b), the resonance cone angle is frequency dependent. One can see from

this equation that lower frequencies will have a smaller resonance cone angle than higher frequencies. In addition, this emission has an upper cutoff, as the resonance cone angle goes to $\theta_{res} = 0$ at either the plasma frequency of cyclotron frequency. These results imply that as a spacecraft flies through a region of whistler mode emission propagating along the resonance cone it will encounter higher frequencies first, and detect lower frequencies only near the midpoint of its pass through this region. This emission will also be bounded on the high frequency end by either the plasma frequency or cyclotron frequency, whichever is lower. A diagram of this is shown in Figure 1(c). The end result is that this emission is will display a characteristic funnel shape when plotted on a frequency versus time spectrogram, as shown in Figure 1(d).

This radio emission, however, is only one part of the larger picture of auroral emissions. Figure 2 shows a basic model for how auroral hiss is generated and how it propagates as it travels away from the planet. As shown in this figure, auroral hiss emission originates from the high-latitude regions of planetary magnetospheres, and is known to be produced by upward-propagating electron beams associated with the aurora. To be clear, auroral hiss emissions can actually be produced by either upward or downward propagating electron beams. However, the detection of such emissions is dependent upon the location of the spacecraft as it orbits the planet. In the case of Cassini, we expect all detected auroral hiss emissions to be upward propagating, simply due to the distance that Cassini keeps from Saturn over the course of its orbit. However, Poynting vector analysis is necessary to prove this assertion.

As this emission propagates away from the planet, it expands outward along a conical surface, centered on magnetic field lines. In addition, field-aligned current structures are often observed, generated by the flow of particles in the planet's magnetic system, which travel in the

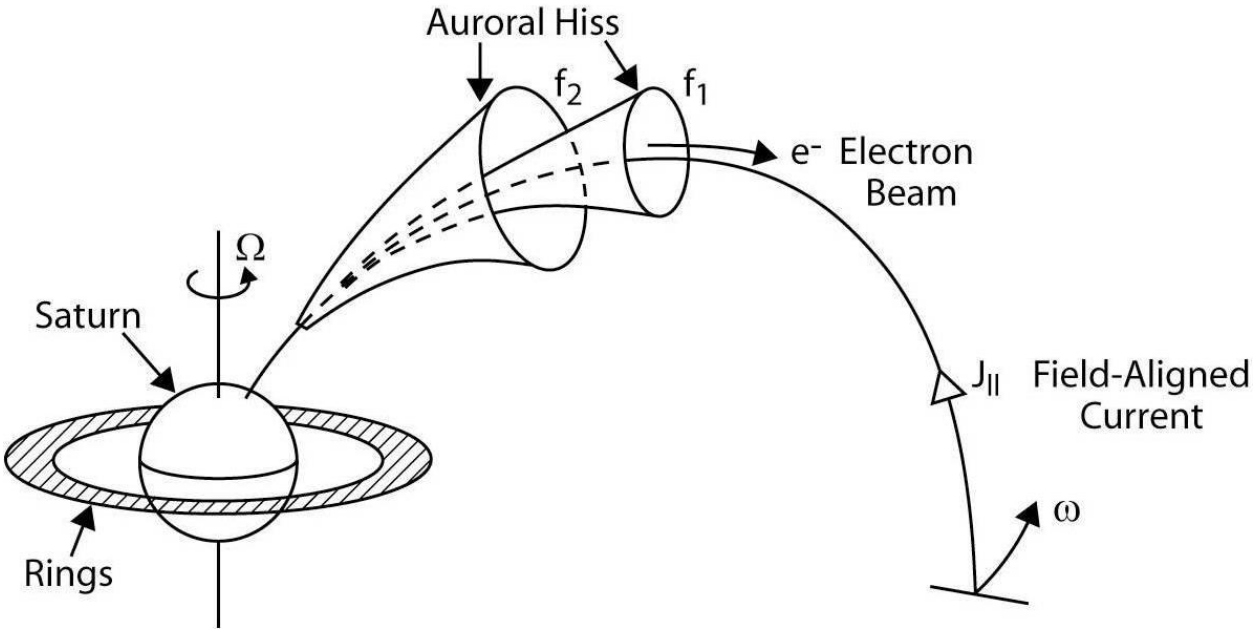

Figure 2 – A basic model of the generation and propagation of auroral hiss. While it has been constructed based on results at Saturn, its principles also apply at Earth.

opposite direction from the electron beams. Finally, the emission may possess a periodicity, the nature of which may provide insight into the source of control of these emissions. This dissertation will provide and discuss observations of these characteristics and others, along with evidence to support the theory of the emission's generation and propagation in the Saturn environment.

CHAPTER 2

BACKGROUND

2.1 Early Work

Cassini is the first spacecraft to orbit Saturn, and has provided the first opportunity to study auroral hiss emissions at the planet. However, although the study of auroral phenomena at Saturn is only a recent endeavor, radio emissions from other planets have been observed for decades. The auroral regions of Earth, including auroral hiss emission, have been studied by satellites for nearly 50 years.

The first reported observations of what we now call auroral hiss, however, were not made by a satellite. These initial detections were made using ground-based very-low frequency (VLF) radio instruments in 1959. *Martin et al.* [1960] discovered a close association between the visible aurora and a very low frequency broad band hiss using a large vertical loop antenna that was designed for the study of whistlers and similar low-frequency phenomena. This study found that visible aurora and low frequency hiss were detected together over 80% of the time, and most of the exceptions were due to weather conditions, such as cloud cover obscuring the visible aurora. Results such as these were influential as space observation became possible, as a number of satellites shortly later would study the auroral regions.

One of the first satellites to study the auroral regions was Injun 3, which was built at the University of Iowa and launched December 13, 1962 [*O'Brien et al.*, 1964]. The instrumentation carried by the satellite would prove to be crucial in increasing our understanding of auroral emissions. Injun 3, which was magnetically oriented to enable auroral studies, carried a series of integrated charged particle detectors, a trio of auroral photometers to measure the visible light

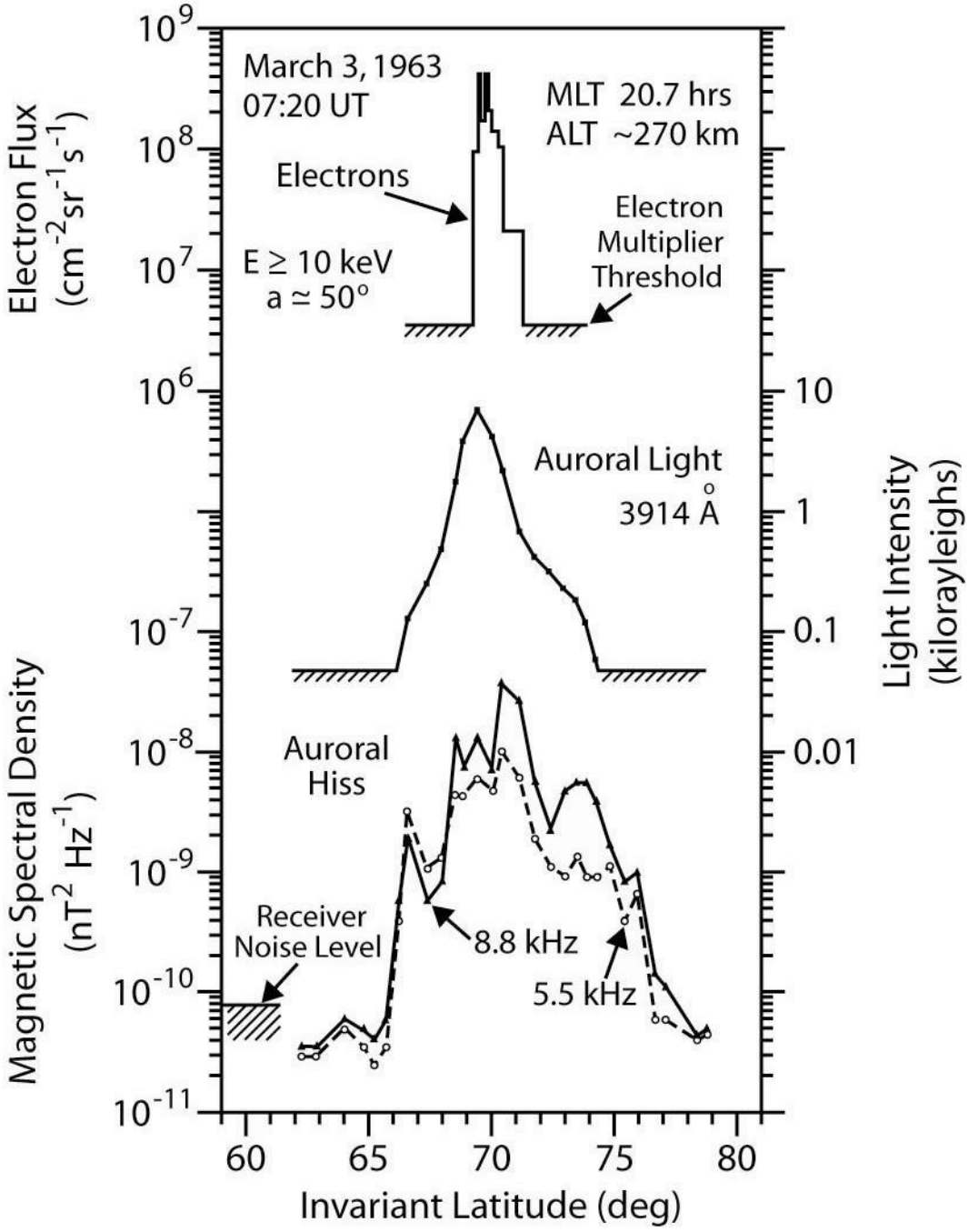

Figure 3 – Data from three different instruments carried aboard Injun 3. When plotted together as a function of time, data from these instruments reveal a correlation in auroral emissions.

intensity of the aurora, and a magnetometer to monitor the magnetic field strength. The results from these instruments formed the foundation for understanding the generation of auroral hiss.

One of the most striking results from Injun 3 came when the data from these three instruments were plotted on the same graph as a function of time, as in Figure 3. The end result was that the sharp peaks in electron flux and light intensity correlated well with auroral hiss intensities. Injun 3 was the first satellite to show this three-aspect connection, and was the first step in developing the modern model of the generation of auroral emissions. *Gurnett* [1966] used this data to make the first quantitative investigation of charged particle fluxes and their association with auroral hiss.

Over five years later, on August 8, 1968, Injun 5 was launched into orbit around Earth. Like Injun 3, Injun 5 was magnetically oriented as it circled the planet. Among its scientific goals was to study the relationship of magnetospheric particles to the aurora. In addition, Injun 5 also carried an instrument to study very low frequency (VLF) radio emission in the ionosphere associated with the flux of particles [*Mosier and Gurnett*, 1969]. An example of these results is shown in Figure 4, a frequency versus time spectrogram, which is color-coded for the propagation direction of the radio emission along the magnetic field. These data provided an early display of what we now recognize as the characteristic funnel-shape emission due to resonance cone propagation, as described earlier.

An important related discovery, as displayed in Figure 4, was that not only was the auroral radio emission correlated with electron flux, but that these emissions were observed to be propagating from both above and below the spacecraft [*Gurnett et al.,* 1971; *Gurnett and Frank*, 1972]. This finding implied that not only were electron beams moving downward to cause the visible aurora, but electrons were also moving upward from the lower ionosphere into the magnetosphere, completing a current system between the ionosphere and magnetosphere. This larger system is detailed in Figure 5.

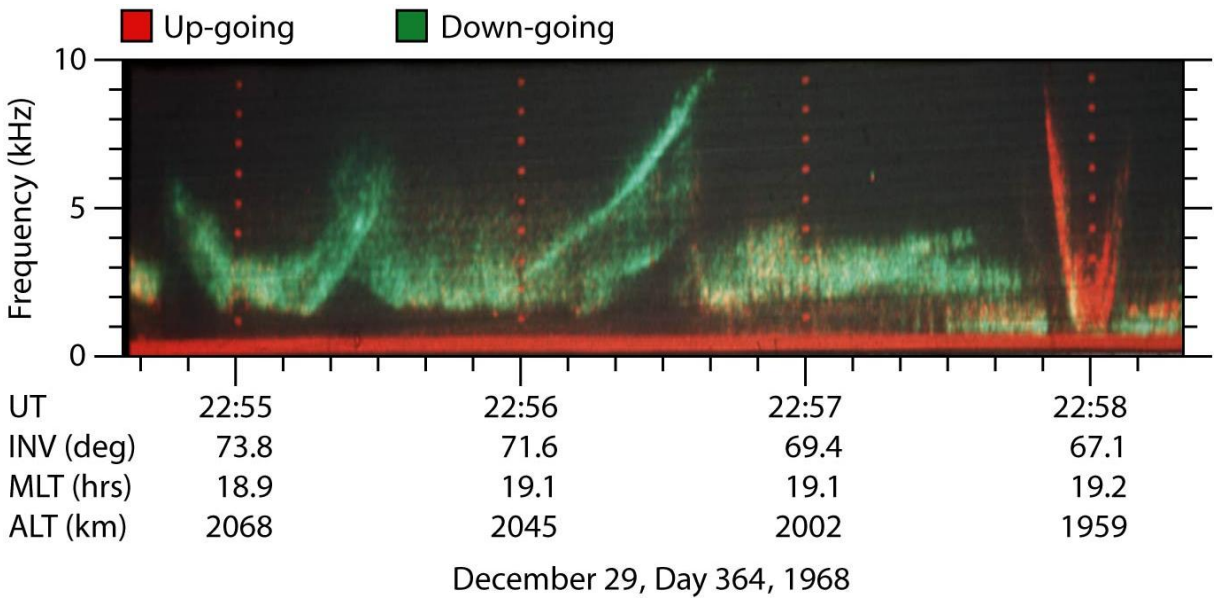

Figure 4 – Data from the Injun 5 spacecraft, color coded for propagation direction. The observation of both upward and downward propagating emission indicates that electrons are propagating in both directions between the ionosphere and magnetosphere.

However, in addition to this demonstrating the propagation in both directions, this figure also reveals two very different ways auroral hiss can appear on the spectrogram. From a more localized source, such as the upward-moving electron beam in Figures 4 & 5, the emission displays more idealized resonance-cone propagation properties, only appearing near the resonance cone and not filling in the interior of the signature on the spectrogram. On the contrary, for an extended source region, the emission is filled in, similar to the downward propagating emission displayed in these two figures [*Santolik and Gurnett*, 2002]. This result is due simply to overlapping resonance cone emission from the multiple sources, causing the interior of the plotted emission to be filled in. Alternatively, the emission can also become filled in as a result of overlapping emission from multiple source regions along a common line of propagation. These two scenarios, however, can be distinguished from one another by the appearance of the vertex of the funnel-shaped signature, as only an extended source will produce

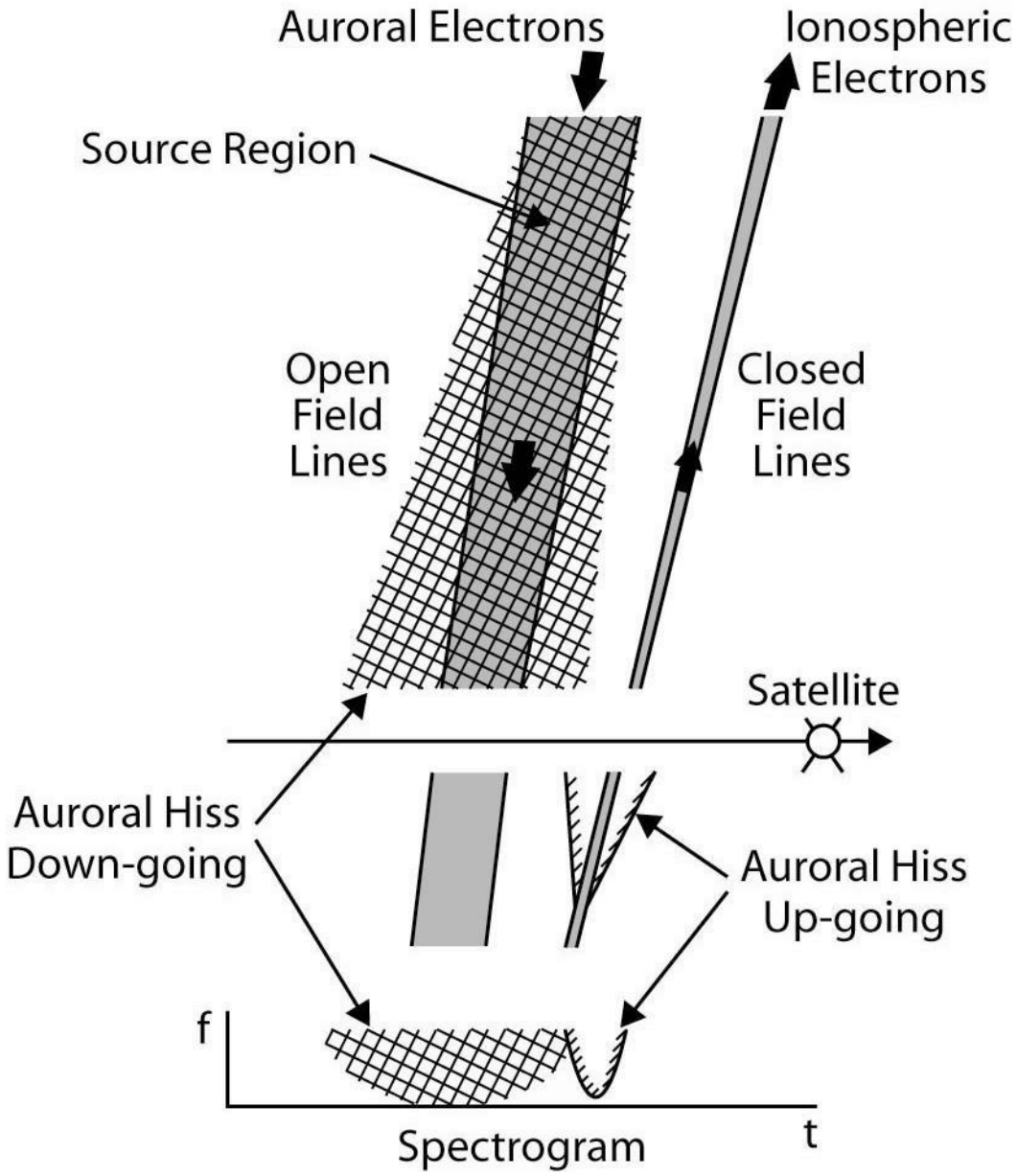

Figure 5 – A model of auroral hiss production, along with the corresponding signatures on a frequency-time spectrogram. The differences in appearance are a direct result of the structure and orientation of the source region, or regions, which produced the emission.

a broad vertex on a spectrogram. A series of point sources would instead produce a sharp vertex at the lowest frequency of the emission. These concepts are illustrated in Figure 5.

2.2 Auroral Hiss in the 1980s

Roughly ten years later, in August of 1981, a two-satellite mission known as Dynamics Explorer was launched. The spacecraft were placed in two different orbits, with DE-1 being in a higher, more elliptical orbit, and DE-2 in a low-altitude circular orbit. Due in part to a rocket malfunction, DE-2 would only orbit Earth for a year and a half before re-entering the atmosphere. DE-1 carried among its experiments the Plasma Wave Instrument (PWI), which measured auroral hiss, auroral kilometric radiation, Z-mode radiation, and narrowband emissions for nearly ten years [*Gurnett et al*., 1983; *Gurnett and Inan*, 1988]. The breadth of data this survey produced allowed for in-depth study of Earth's auroral regions.

Dynamics Explorer spectrograms, which display PWI data, are similar to those used to display and study Cassini RPWS data. As a result, they serve as a useful tool for comparison between Earth and Saturn when studying auroral emissions. An example Dynamics Explorer spectrogram is shown in Figure 6. Many of the characteristic signatures are easily observed, particularly the funnel-shaped emission. The asymmetry of the funnel can be explained by both the trajectory of the orbit and the presence of Landau damping [*Morgan et al.,* 1994]. These funnels were often observed in correlation with upward electron beams [*Lin et al.*, 1984].

All of these spacecraft played their part in observing the natural auroral emission that occurs at Earth, and their combined results largely developed today's models of the processes that occur in the auroral regions that drive the different types of emission that appear there. Still, despite the substantial understanding of auroral processes that had been gained through these observations, there had been no direct test of the theory through experiment, and such conditions would have been highly difficult to recreate in laboratories on Earth with the technology available at the time. However, the development of the space shuttle presented a unique

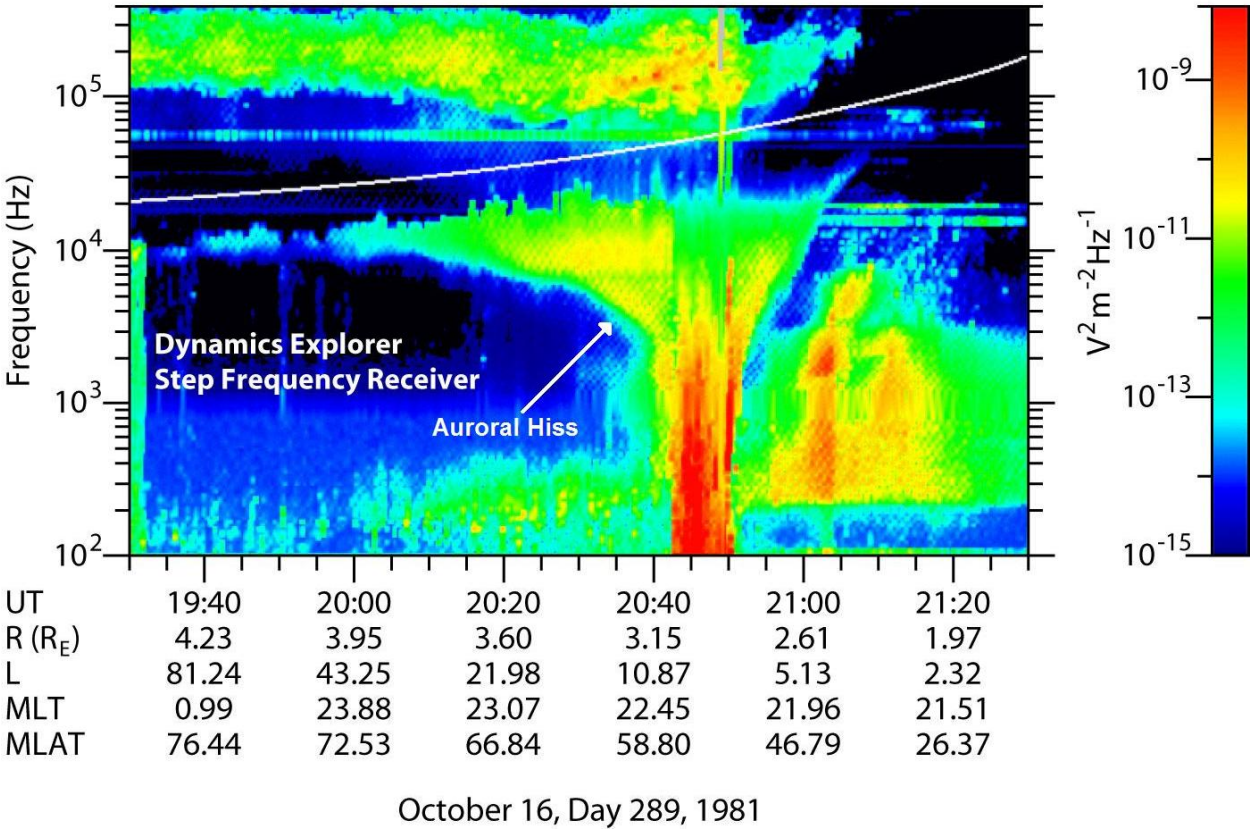

Figure 6 – A spectrogram from Dynamics Explorer, showing the characteristic funnel-shaped emission of auroral hiss. The white line represents the electron cyclotron frequency. With its similarities to the RPWS experiment aboard Cassini, DE is a useful tool for comparing the emissions of the two planets.

opportunity to test the theory first-hand by attempting to artificially create the conditions believed to generate auroral hiss with an onboard experiment.

This theory would be put to the test by the space shuttle *Challenger*, which lifted off for mission STS-51F on July 29, 1985. The primary payload for the mission was Spacelab-2; however, the shuttle also carried a spacecraft built at the University of Iowa called the Plasma Diagnostics Package (PDP). The PDP carried several instruments designed for studying the ionospheric environment and plasma parameters in the vicinity of the shuttle, and how they were affected by the shuttle's presence [*Kurth and Frank*, 1990].

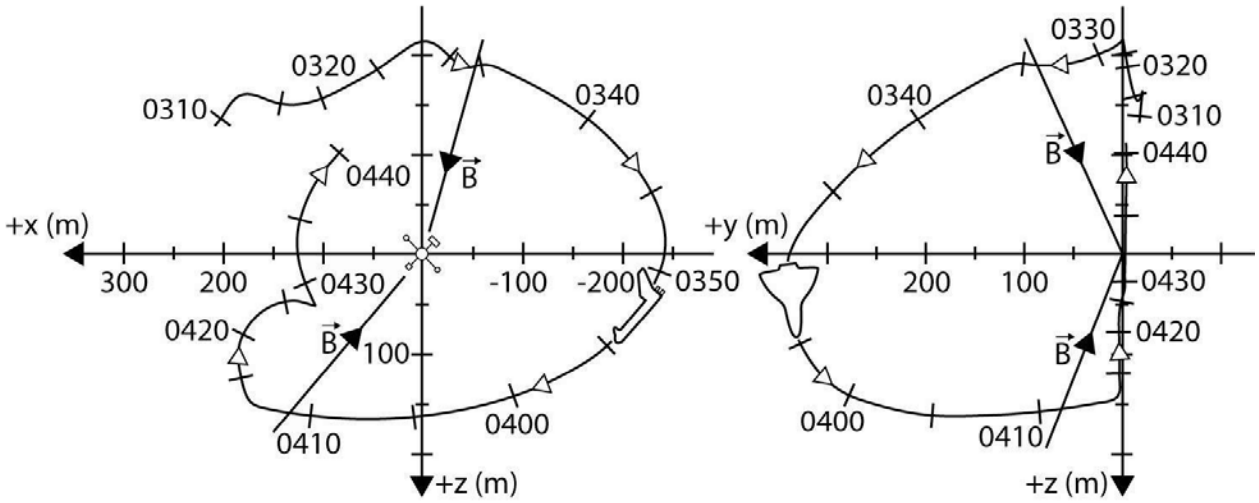

Figure 7 – Orbital path followed by the space shuttle *Challenger* around the Plasma Diagnostic Package (PDP). The two times where the shuttle and PDP fell along a common field line were used to test the theory of auroral hiss generation.

However, the PDP was also used in an attempt to simulate auroral hiss emission in order to test the now long-standing theory of its generation. After releasing the PDP, *Challenger* orbited around the package for a few hours. A map of the orbital path is shown in Figure 7. *Challenger* also carried an electron gun on board, which was pointed toward the PDP. If the theory on auroral hiss was accurate, the PDP would register the characteristic funnel shape auroral hiss-like emission whenever the line between the electron gun and PDP coincided with the direction of a magnetic field line.

As can be seen from Figure 7, there were two times where the space shuttle's electron beam coincided with the magnetic field direction, as marked by the arrows in both panels. One of the two times where this emission was expected to be observed was at 3:34 UT. The observed electric field intensities from around this time are shown in Figure 8, and discussed in detail by *Gurnett et al*. [1986]. As expected, a remarkably clear funnel of emission was observed at this time, lending credence to the theory of auroral hiss generation. The electron beam, when moving

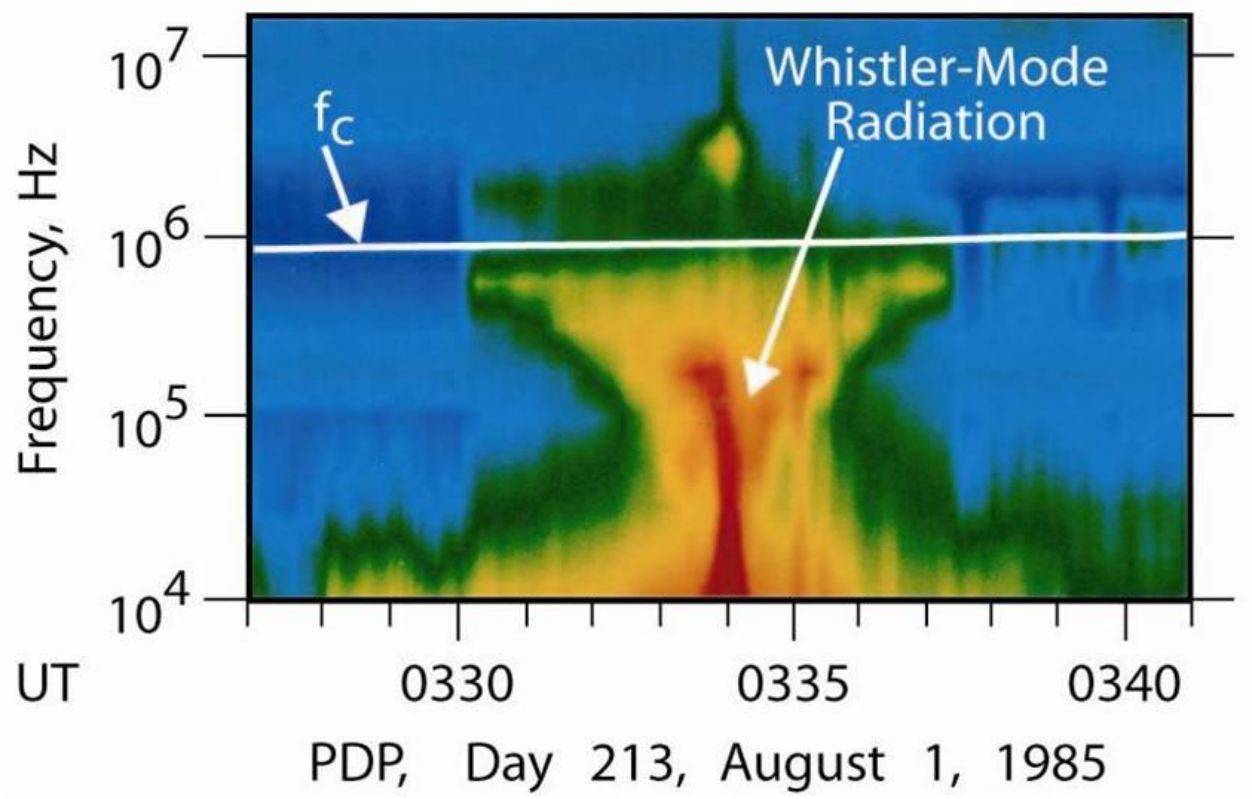

Figure 8 – Result of the PDP experiment, which produced auroral hiss-like emission. The intense emissions are centered on the time where the shuttle and PDP fell along a common magnetic field line.

along the magnetic field line, had produced radiation which matched the characteristic signature of auroral hiss.

2.3 Recent Work

Some of the most recent study of Earth's auroral regions has been performed by the Fast Auroral SnapshoT Explorer (FAST) [*Pfaff et al.*, 2001]. FAST was launched in August of 1996, and continues operations to this day. Following a highly elliptical path, FAST crosses the auroral zones four times each orbit, and collects high-resolution "snapshots" while in these regions. Instruments aboard the satellite are capable of measuring the electric and magnetic

fields, plasma waves, energetic particles, ion mass composition, and plasma density and temperature, all with unprecedented resolution. These capabilities provide a very comprehensive study of this region.

Among the results from FAST is the study of "very low frequency (VLF) waves" or "VLF saucers", which is corresponding terminology to what we refer to as auroral hiss. Observations of the waves and particles associated with this emission reveal that roughly 85% of these detections are generated by upward-propagating electrons in the downward current region of the aurora [*Ergun et al.*, 2003]. This work also found that electron phase-space holes at the emission's vertex were observed nearly all the time in conjunction with these detections, which has been interpreted to show that the source region of these emissions is located in or near parallel electric fields in the downward current region of the aurora.

The FAST satellite carries instruments capable of detecting several aspects of auroral hiss emission, and as a result has provided striking findings while studying this phenomenon at Earth. An example of this is shown in Figure 9, from *Ergun, et al.* [2003]. The first two panels, (a) and (b), represent the electric field and magnetic field intensities respectively in the direction perpendicular to the spin plane. The negative electric field signal in (a), followed by the positive region, corresponds to a diverging electric field structure, indicating a downward parallel electric field is present on the flux tube of the spacecraft at a lower altitude [*Ergun et al.,* 1998]. Similarly, in (b), the regions of negative slope represent upward field-aligned currents, assuming a sheet-like current structure, while positive regions correspond to downward currents. The steep negative slope in the region of interest (roughly 3:25 UT to 3:35 UT) indicates the presence of a downward field-aligned current, to go along with the downward-directed parallel electric field that was inferred from panel (a).

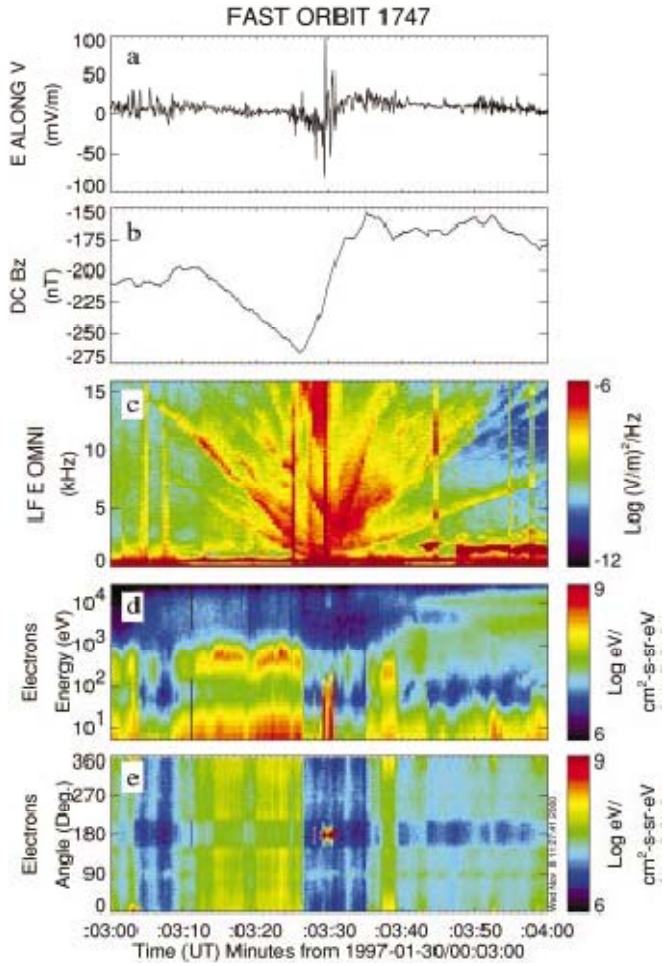

Figure 9 – From *Ergun, et al*. [2003], showing correlation between (a) perpendicular electric field in the spin plane, (b) ΔB along the spacecraft spin axis, (c) electric field spectral power density, (d) electron differential energy flux versus energy, and (e) versus pitch angle. This multi-instrument display provides a comprehensive look at auroral hiss emissions.

Furthermore, the resolution in the last three panels of Figure 9 allows for very specific knowledge of the inner aspects of this radiation. In panel (c), the funnel-shaped nature of auroral hiss can be observed in a broad sense, but the very high band resolution allows distinct "arms" of emission to be defined as well. At least 16 distinct "arms" can be identified, corresponding to eight or more three-dimensional source regions, though it is not possible to pair the arms unambiguously without an accurate density profile. Using the slopes and bandwidths of each

arm, the source regions were determined to each extend less than 10 km in latitude and altitude, and longitudinal sizes on the order of a few tens of kilometers. The sources were at varying distances, though all were on the order of hundreds of kilometers from the spacecraft. Finally, the last two panels, (d) and (e), plot the electron intensities against energy and pitch angle, respectively. These two plots demonstrate that at the vertex of the emission, the spectra is dominated by intense, low-energy, up-going electron fluxes, which are aligned with the magnetic field in their propagation.

FAST has also produced data that suggest a role for the ions present in these regions. Downward flowing ion beams (DFI) have been frequently observed by FAST, and have been characterized as a horseshoe-shaped distribution consistent with acceleration in a parallel potential drop, followed by motion into a region of increased magnetic field strength [*Klumpar et al.*, 1999]. FAST observes these ion beams frequently in conjunction with electron beams and the corresponding "VLF saucer" emission [*Cattell et al.*, 2002], indicating ion detections may be a common player in these regions, even though they are not known to have any role in the generation of this emission.

Although most of the study of auroral hiss has been performed at Earth, similar detections have also been made at Jupiter. In 2001, the Galileo spacecraft made a close flyby of Jupiter's moon Io, and detected whistler-mode emission with characteristics similar to Earth's auroral hiss, as reported by *Xin et al.* [2006a]. Assuming propagation along the resonance cone, *Xin* used ray-tracing analysis to map the emission back to its source. This study found that the radiation originated very close to the surface of Io, and ultimately led to the conclusion that this auroral hiss emission was generated by an electron beam that was part of the field-aligned current system induced by Io as it interacted with the rapidly rotating magnetosphere of Jupiter.

With auroral hiss emission having been detected at Saturn for the first time, similar research to that at Earth and Jupiter has been performed. The purpose of this research has been to study and test this overall model of auroral hiss emissions, to gain an understanding of its finer details and deviations from the simplified ideal models, and to draw comparisons to the similar emissions observed at Earth. In order to perform such a study, a multi-instrument perspective was required, and this research made use of data collected by several Cassini instrument investigations. These instruments and their capabilities will be described in Chapter 3.

2.4 Theory of Emission Generation

Over the last 50 years, auroral hiss has been well studied at Earth by various ground-based and space-based instruments. Consequently, general theories about the generation and propagation of auroral hiss emissions have been well-formulated and are widely accepted throughout the scientific community. The theory includes a variety of different components, which are part of the larger system of the planet's magnetosphere. Still, while this theory is well established at Earth, it remains to be seen whether or not it translates well when applied to the environment present at Saturn.

Auroral hiss originates from the high-latitude regions of planetary magnetospheres, and is known to be produced by electron beams associated with the aurora. Several authors have attempted to explain how such a beam can generate auroral hiss. A number of early theories were based on generation by an incoherent Cherenkov mechanism [*Ellis*, 1957; *Jorgensen*, 1968]. Cherenkov radiation is produced when the index of refraction of a medium is such that a charged particle can move faster than the phase velocity of a wave. This condition is satisfied for the whistler mode, as the index of refraction becomes very large when approaching the

resonance cone. However, this theory was rendered unviable after *Taylor and Shawhan* [1974] showed that the observed intensities of auroral hiss emission were far too large to be explained by an incoherent mechanism. They concluded instead that these emissions must be generated by a coherent mechanism, such as a plasma instability.

Around the same time, sounding rocket experiments observed whistler mode plasma waves in conjunction with an artificially injected electron beam. The Electron Echo 1 experiment carried an electron accelerator to an altitude of 350 km, injecting the Earth's magnetic field with a series of 16-ms pulses of electrons [*Cartwright and Kellogg*, 1974]. Onboard antennas and receivers measured the electric field of waves generated by these beams, including those at the lower-hybrid resonance (LHR). The amplitude of emissions at the LHR frequency could only be produced by an instability or coherent emission. Similarly, Electron Echo 2 detected whistler mode waves associated with these electron injections [*Monson et al.*, 1976]. These results showed a strong correlation of the wave intensity with the electron beam intensity, which were injected on two different time scales at multiple pitch angles. These results rendered strong experimental support for the conclusions of *Taylor and Shawhan*.

Shortly after the determination that a coherent mechanism must be at the root of the beam acceleration, an effort was made to bridge the gap between the early work and these recent discoveries and conclusions. VLF hiss was soon proposed to result from convective beam amplification of incoherent Cherenkov whistler mode radiation by the beam of precipitating auroral electrons [*Maggs*, 1976]. Such amplification could occur in the environment around the Earth, where beam-plasma instability in the inhomogeneous ionosphere would amplify the incoherent radiation. That study performed calculations using various reasonable (physical) velocity distributions for the beam, which showed that this model could account for the power

spectrums observed by the satellite instruments. Furthermore, its use of the wave kinetic equation helped to determine the important geometric parameters and frequency regimes where non-linear processes would be important.

With the knowledge that a beam-plasma instabilities could produce the emission, the final related question was which instability was the source. Since auroral hiss is propagating near the whistler mode resonance cone, the emission is quasi-electrostatic, and has a very small phase velocity, much less than the speed of light. As a result, it was believed that the emission is produced by a beam-plasma instability associated with the Landau resonance. This would later be demonstrated by nonlinear computer plasma simulation [*Farrell et al.,* 1989]. Landau theory states that when the phase velocity is in a region of positive slope on a velocity plot of the plasma distribution function, instabilities develop that then excite a wave. A summary of this is shown in Figure 10. This wave is unstable, and gains energy at the expense of the particles generating it, growing the wave. The Landau resonance involves interactions with particles travelling in the same direction as the wave, which implies that the direction of propagation for the electron beam must be the same as the direction of propagation of the whistler-mode hiss.

Recent results provided by results from the FAST satellite have added additional confirmation to this theory. Quantitative comparisons of electric field strengths and ion beam energies observed with FAST suggest a quasi-static parallel potential structure in the auroral regions [*Carlson et al.,* 1998]. Parallel electric fields in diverging electric field structures are found to be accelerating auroral electrons upwards, while converging electric field structures are responsible for accelerating the downward-flowing electrons that produce the visible aurora. In both cases, these electrons have been determined to carry the field-aligned currents required and observed in the system.

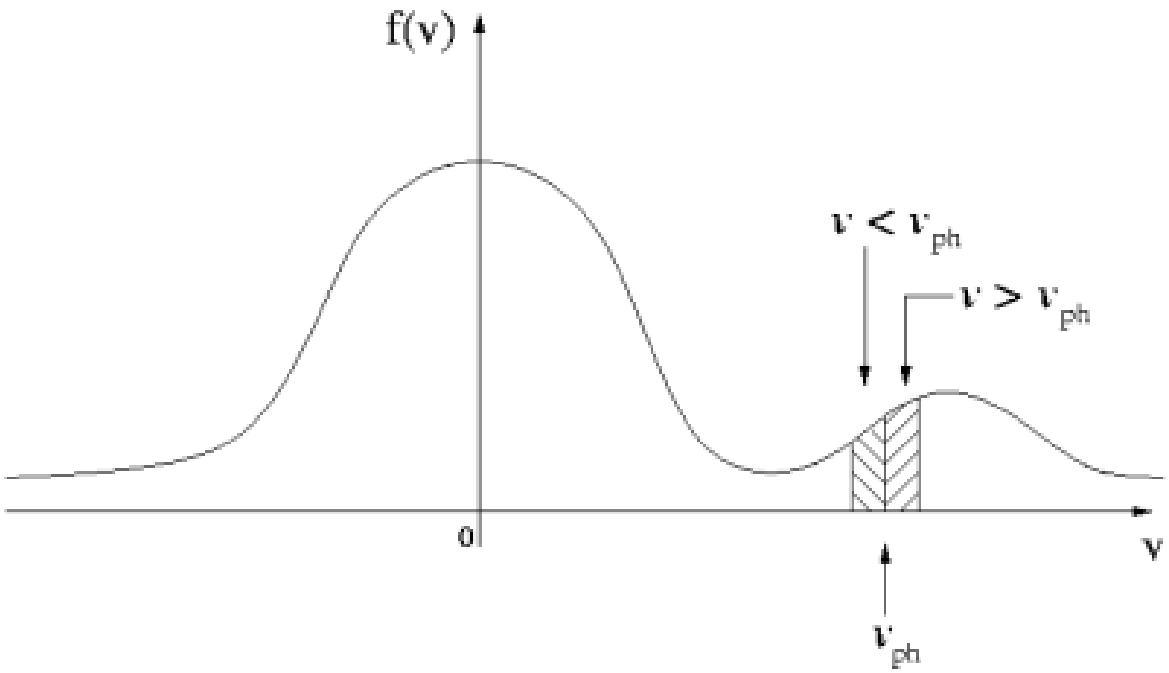

Figure 10 – A bump-on-tail distribution. When the phase velocity is in the region of positive slope, it produces an instability that excites a wave. This wave grows at the expense of the particles, which lose energy to the wave as they settle into a stable distribution.

At Saturn, the current system is more complicated than that observed at Earth, but the same basic concepts are believed to apply. The observation of a rotating plasma disk structure around Saturn requires the presence of a more complex current structure, consisting of not only up-going and down-going currents like those observed at Earth, but also current structures through the plasma disk itself, as required to balance the forces of the system. However, since the series of currents is largely prevalent only at lower latitudes, and the ring currents concentrated in the equator, the auroral regions remain largely unaffected by this change, suggesting Earth-like mechanisms for beam generation.

CHAPTER 3

THE CASSINI SPACECRAFT

Figure 11 – Cassini instrument configuration. Image credit – NASA.

3.1 RPWS

The Cassini spacecraft carries twelve instruments, along with six others that were on the Huygens Probe, which are positioned as shown in Figure 11. For this research, the primary instrument used will be the Radio and Plasma Wave Science (RPWS) instrument, which is capable of detecting auroral hiss radio emission. RPWS is made up of four major components:

the magnetic search coil sensor assembly, the electric field sensor, the Langmuir probe sensor assembly, and the instrument main electronics, which control the instrument function and process the signals received by the various sensors.

The magnetic search coil sensor assembly is made up of three magnetic search coil antennas and an associated preamplifier, and makes measurements of the magnetic component of the emission. This sensor assembly operates over a range of 1 Hz to 12 kHz, and is defined to be oriented in such a way as to measure the B_x, B_y, and B_z components of the magnetic field. The electric field sensor is made up of three deployable monopole field antenna elements, an associated preamplifier, and the deployment electronics. These 10-meter antennas, which operate at frequencies between 1 Hz and 16 MHz, are oriented differently than the magnetic search coils, and are generally labeled as the E_u, E_v, and E_w components. The Langmuir probe sensor assembly consists of a sensor, a preamplifier, and associated control electronics. The probe sensor is a 5-cm diameter sphere positioned at the end of a 1-meter rod, and is used to measure the currents and potentials in the surrounding plasma, which can be interpreted to determine the electron density and temperature. All of these components have been utilized in this research.

The signals from the RPWS antennas are processed by five receiver systems, though only three of them have been relevant to this research. The low-frequency five-channel waveform receiver provides high-resolution spectral measurements of both the electric and magnetic components in the frequency range from 0.1 Hz to 2.5 kHz, the frequency regime where auroral hiss is generally observed. The medium-frequency receiver operates from 25 Hz to 12.6 kHz, also overlapping the frequency range of auroral hiss, but extending up to higher frequencies as well. Finally, the wideband receiver obtains very-high-resolution waveforms for selected time

intervals. For a complete description of the RPWS instrument and its components, see *Gurnett et al*. [2004].

3.2 MAG

Magnetic field measurements are provided by the Dual-Technique Magnetometer (MAG). MAG has two main sensors: the vector/scalar helium magnetometer and the fluxgate magnetometer. The vector/scalar helium magnetometer (V/SHM) was supplied by NASA's Jet Propulsion Laboratory and is used to make both vector and scalar measurements of Saturn's magnetic field. The fluxgate magnetometer (FGM) was provided by Imperial College in London and is used to make vector field measurements. Since magnetometers are sensitive to currents, they must be mounted as far away from the spacecraft's primary electronics as possible. As a result, both instruments are mounted on Cassini's magnetometer boom, with FGM halfway out from the spacecraft, and V/SHM at the very end of the boom. A full description of the magnetic field investigation can be found in *Dougherty et al*. [2004].

3.3 MIMI

The Magnetospheric Imaging Instrument (MIMI) uses three different detectors to study the plasma environment at Saturn. The Low-Energy Magnetospheric Measurements System (LEMMS) measures low-energy proton, ion, and electron angular distributions. LEMMS is mounted on a scan platform capable of 180-degree rotations, so as to allow LEMMS to always be pointing in a useful direction regardless of Cassini's orientation. The Charge-Energy-Mass Spectrometer (CHEMS) measures the charge state and composition of ions in Saturn's magnetospheric plasma. Finally, the Ion-Neutral Camera (INCA) is designed to study both

charged and uncharged particles in the magnetosphere. INCA measures three-dimensional distributions, velocities, and rough compositions of magnetospheric ions. INCA also captures remote images of the global distribution of energetic neutrals in the magnetospheric plasma, and can measure composition and velocities for those particles as well. More on MIMI can be found in *Krimigis et al*. [2004].

3.4 CAPS

Finally, the Cassini Plasma Spectrometer (CAPS) investigation detects low-energy electrons and ions. The electrons are detected by the Electron Spectrometer (ELS), which measures the flux of electrons as a function of energy per charge and aperture entry direction over 63 different energy steps. These results can be manipulated to obtain the flux as a function of energy and pitch angle, which is more useful generically since these values are independent of the spacecraft orientation. Since electrons are known to be the source of the auroral hiss emission, the ELS instrument has been the primary particle detector used for this research.

Since ions have variable mass depending on their composition, CAPS also has two ion detectors. The first, the Ion Mass Spectrometer (IMS), provides measurements of the flux of positively charged atomic and molecular ions, again both as a function of energy per charge and aperture entry direction. These measurements are species resolved with the aid of a spectrum analyzer module (SAM), which bins the detected ions according to a set of pre-selected channels associated with different ion species, allowing the composition of the detected ions to be determined. Along with IMS is the Ion Beam Spectrometer (IBS), which measures the flux of all positively charged ions independent of their mass. These two instruments together give a complete picture of the detected ions in Saturn's magnetosphere. CAPS also contains an

actuator, which allows these detectors to be rotated over 184 degrees, allowing CAPS, like MIMI, to be pointed in a desired direction for particle observation. The CAPS investigation is described fully in *Young et al*. [2004].

CHAPTER 4

CASSINI OBSERVATIONS & ANALYSIS

4.1 Overview

The Cassini spacecraft was launched on October 15, 1997, and after a series of gravity assist flybys, including two of Venus, one of Earth, and one of Jupiter, Cassini arrived at Saturn on July 1, 2004. The mission of the Cassini spacecraft is to investigate Saturn, its rings, moons, and magnetosphere [*Matson et al.,* 2002]. Although the Cassini spacecraft arrived at Saturn in the middle of 2004, the first few years of its mission focused heavily on flybys of Saturn's many natural satellites, which require the spacecraft to follow orbital paths along the equatorial plane. As a result, Cassini remained in a low-latitude orbit for more than its first two years, preventing the study of the auroral regions and most of the related emissions.

Cassini's orbit did not reach a sufficient inclination to study these regions until September 26, 2006, when it began a series of inclined orbits. Not long after entering the auroral regions, Cassini made its first detections of Saturn's auroral hiss. Cassini maintained these inclined orbits until May 26, 2007, after which it returned to lower latitude orbits to accommodate additional moon flybys. Cassini returned to the auroral regions for a second time on January 1, 2008, and remained in this high-latitude orbit until beginning its descent toward the equatorial plane on July 31, 2009, where it remains today. During these two intervals, Cassini's orbit was sufficiently inclined to reach high magnetic latitudes (>30 degrees), allowing the RPWS instrument to make auroral hiss measurements. While the first series of high-inclination orbits only reached a latitude of about 60 degrees, the second series moved as high as about 75 degrees, allowing study of the full region. A plot of Cassini's orbits from its arrival to

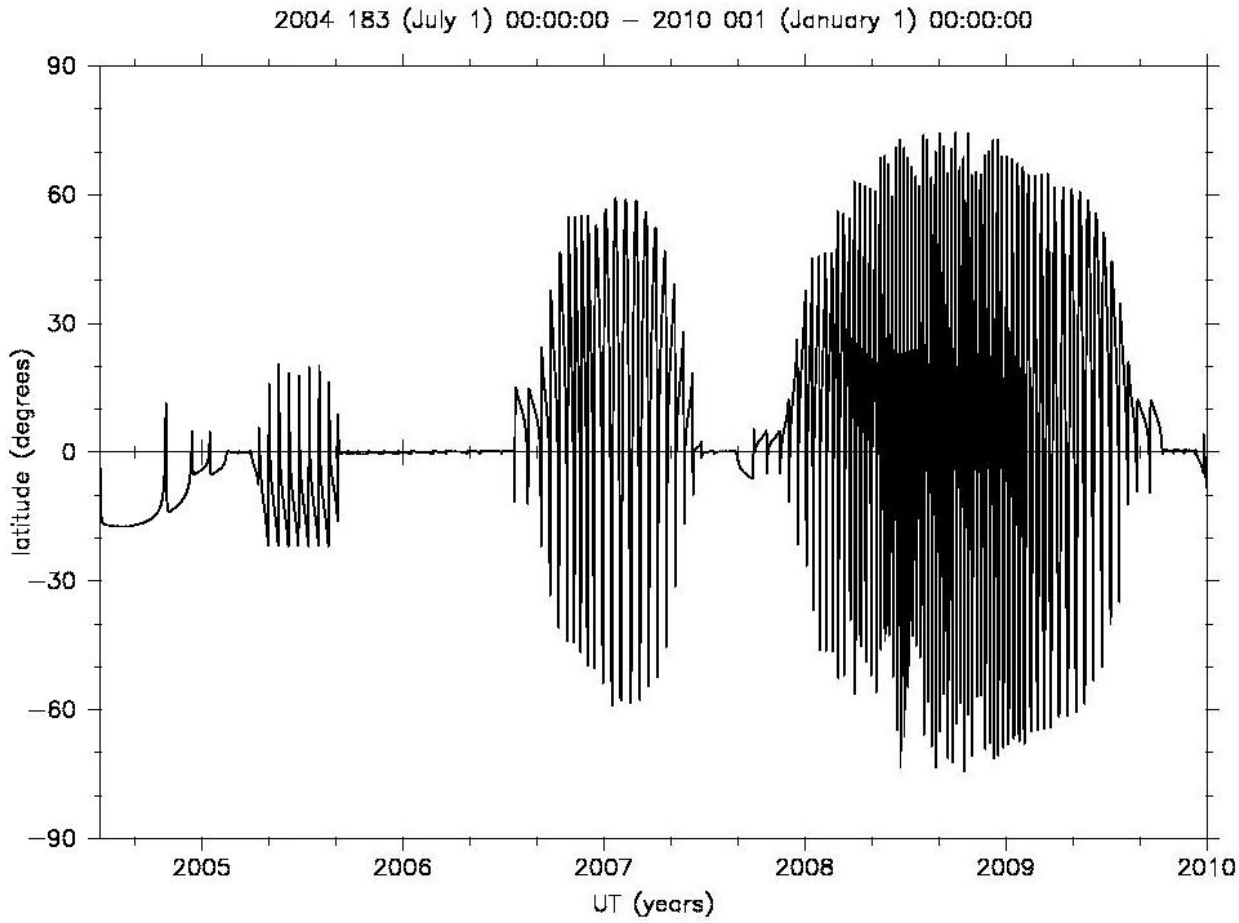

Figure 12 – Latitudinal map of Cassini's orbits from 2004 arrival through 2009. Cassini has reached high latitudes in two intervals during its mission, allowing for the study of the auroral regions at Saturn.

the start of 2010 is shown in Figure 12. As anticipated, once Cassini was in a region where detection of these emissions was possible, such observations were made.

Figure 13 shows a frequency-time spectrogram of an auroral hiss event observed by Cassini. This spectrogram is a pristine example of Cassini observations, and shows most all of the typical features observed in this frequency range. This event clearly displays the typical funnel shape spectrum generally observed with auroral hiss, the characteristic signature of this emission, as a result of its resonance cone propagation. Although many detections of auroral

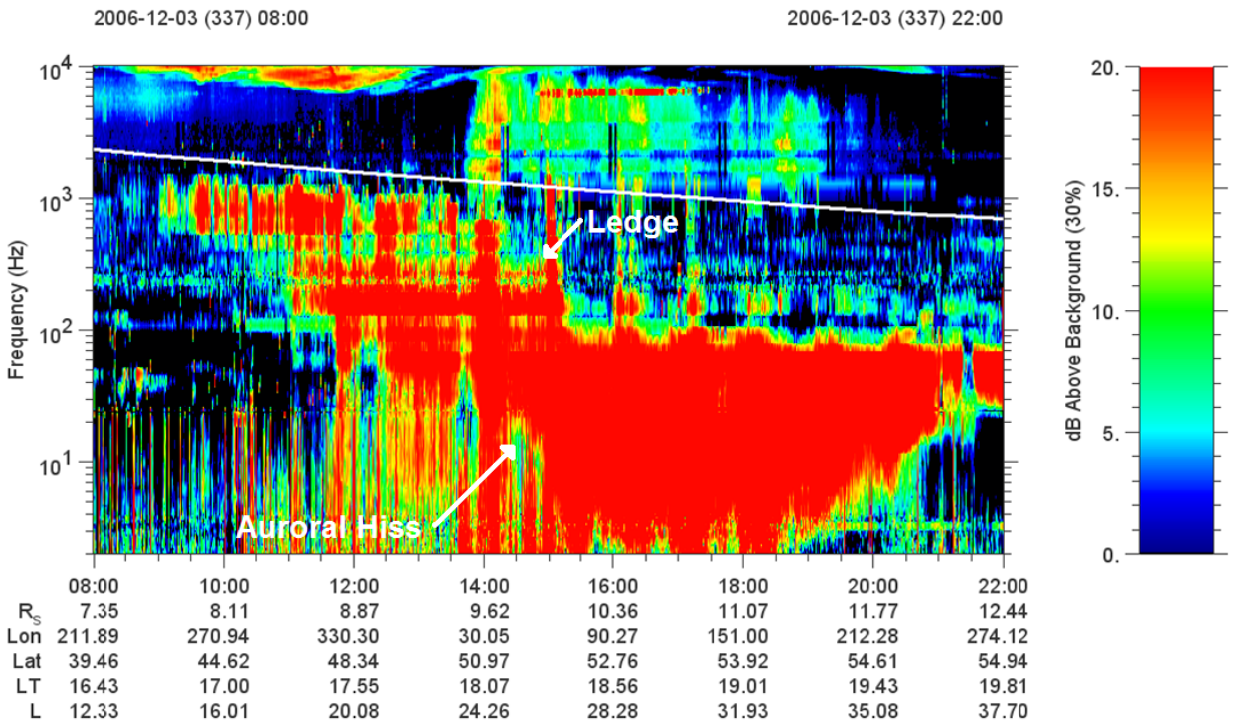

Figure 13 – A characteristic Cassini RPWS spectrogram of auroral hiss emission, displaying the V-shaped funnel associated with this emission, as well as the ledge-like step on its lower-latitude edge. The white line near 1 kHz represents the electron cyclotron frequency.

hiss by the RPWS instrument are not as well-defined as this one, most still display the basic funnel-shaped characteristic that is associated with this emission.

As described in Chapter 2.1, the appearance of the auroral hiss emission, as in Figure 13, allows for the determination of basic properties of the source region, in particular its orientation. Since the base of the example emission in Figure 13 does not have a sharp vertex, instead appearing very broad, the source region of the emission likely has an extended size along the direction of travel of Cassini. Furthermore, since the emission is filled in instead of just outlined, it should be formed by the sum of a series of resonance cone-style propagations along the direction of propagation, indicating the source is also extended in altitude.

One other feature that should be noted in the spectrogram in Figure 13 is the ledge-like step that occurs at roughly 14:00 UT. This step is also a characteristic feature observed in RPWS spectrograms, appearing nearly every time auroral hiss is observed. The step is always oriented such that the emission can be observed at higher frequencies on the equatorward (lower-latitude) side of the emission, but then displays a step down in the upper frequency cutoff with increasing latitude. Since the emission in these higher latitudes displays an abrupt cutoff well below the electron cyclotron frequency, the electron plasma frequency is assumed to be the lower of the two frequencies, and the one which defines the maximum frequency of the emission in these cases. It follows that the observed step reflects a sudden drop in the density on the order of two orders of magnitude.

One possible explanation is to suggest the presence of a plasma cavity, which was commonly observed at Earth by Dynamics Explorer. In the DE data, the center of the auroral hiss emissions, that is to say near the magnetic field lines, commonly had significantly lower plasma densities [*Persoon et al.*, 1988]. Flanked by regions of higher density, these results were indicative of a plasma cavity, a region of diminished plasma presence. However, the density data from various Cassini instruments, including the Langmuir Probe and the CAPS instrument, indicate a considerably different picture at Saturn. In this case, the density profiles do not show a contained region of plasma density. Instead, the higher density region always appears only on the lower latitude side, with a drop-off coinciding with the ledge-like feature on RPWS spectrograms. This instead suggests the presence of a region of higher density at lower latitudes or, more accurately, lower L-shells, not unlike the plasmasphere at Earth [*Gurnett et al.,* 2010]. This observation will be detailed further in Chapter 4.4.

4.2 Location

When studying this emission, one important aspect to check is the location of the observations, with respect to both latitude and local time. If indeed this emission is auroral hiss propagating outward from the auroral regions, it should only be observed at high latitudes, with the centered axis of the funnel more or less following the magnetic field line when Cassini is relatively close to the planet. Indeed, auroral hiss can be detected at lower latitudes as the field lines wrap around toward the equator, due to the funneling, and will also deviate from the field lines at this point as it propagates. However, by this time the emission is considerably more diffuse, making such observations much less likely. Also, this emission should show no preference in to any local time, since Poynting vector analysis has shown this emission to be upgoing from Saturn. As a result, this emission is known to be generated lower in the magnetosphere, not from the solar wind.

An example of this Poynting analysis is shown in Figure 14. Here, the direction of propagation is computed for the auroral hiss funnel that was shown in Figure 13. The top panel displays the sum of the magnetic components, which the middle panel shows the sum of the three electric components, as observed by the magnetic search coil sensor assembly and the electric field sensor, respectively. It can easily be seen that the magnetic detection is far weaker than the electric components. However, this is not an unexpected finding, as auroral hiss is known to be quasi-electrostatic due to its resonance cone propagation. While this renders Poynting analysis difficult, there is generally enough of a magnetic component to give an indication of the direction of propagation. The bottom panel of Figure 14 displays this result, which indicates that the emission is propagating roughly parallel to the magnetic field. Since the field is upgoing from Saturn in the northern hemisphere, the emission is upward propagating.

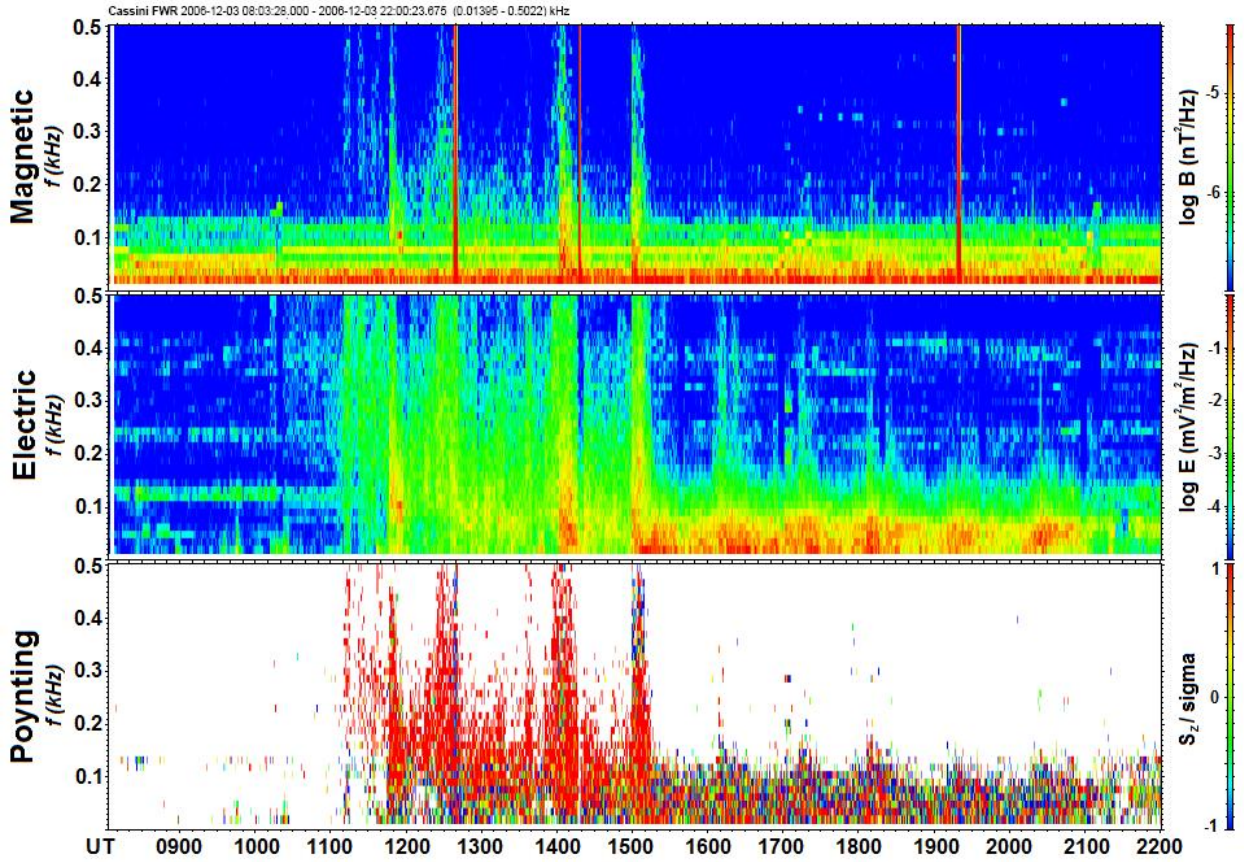

Figure 14 – Poynting vector analysis of the auroral hiss funnel shown in Figure 13. The top panel displays the sum of the magnetic components of the emission, while the middle panel shows the sum of the electric components. The resulting Poynting vector in the bottom panel is directed parallel to the magnetic field, which in the northern hemisphere is upward propagating.

Figure 15 shows a pair of polar plots showing auroral hiss detection. The image on the left plots the detections with respect to local time at Saturn, where the Sun is in the direction of local noon (12 LT). The second image, on the right, is a meridian plane plot with respect to latitude, which ignores the local time of the observation. In both cases, all Cassini orbit trajectories are traced out in green. Subsequently, black dots are overlaid on top of the green whenever an auroral hiss detection is made. These two plots include data from September of 2006 through March of 2008, which includes the first period where Cassini was in high-latitude orbits as well as a series of lower-latitude passes. In both cases, the expected result is illustrated.

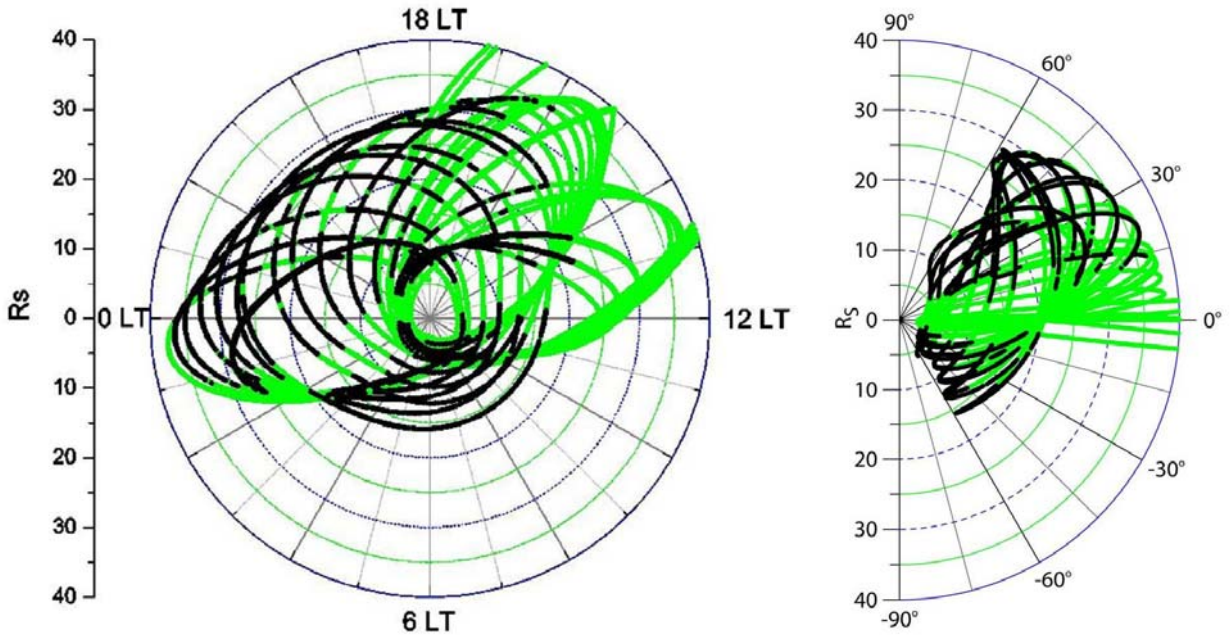

Figure 15 – Auroral hiss detections with respect to local time (left) and latitude (right), from Cassini's first series of high-latitude orbits. Black dots are overlaid on the green dots to indicate the locations where Cassini observed auroral hiss.

Detections are made at all local times, and are largely confined to the higher latitudes, except at large distances from Saturn. Interestingly, in the latitude plot on the right, the equatorward funneling effect can be somewhat observed, particularly in the detections in the southern hemisphere, though in the case of both plots the gaps are largely due to a selection effect from the spacecraft's trajectory.

4.3 Periodicity

In periods where Cassini has been at high magnetic latitudes for extended durations of time, a periodicity appears in the auroral hiss emission. Figure 16 displays a seven-day period of data, over which Cassini was constantly in the high magnetic latitudes of the northern hemisphere. A clear modulation can be observed in the auroral hiss emissions, which is on the

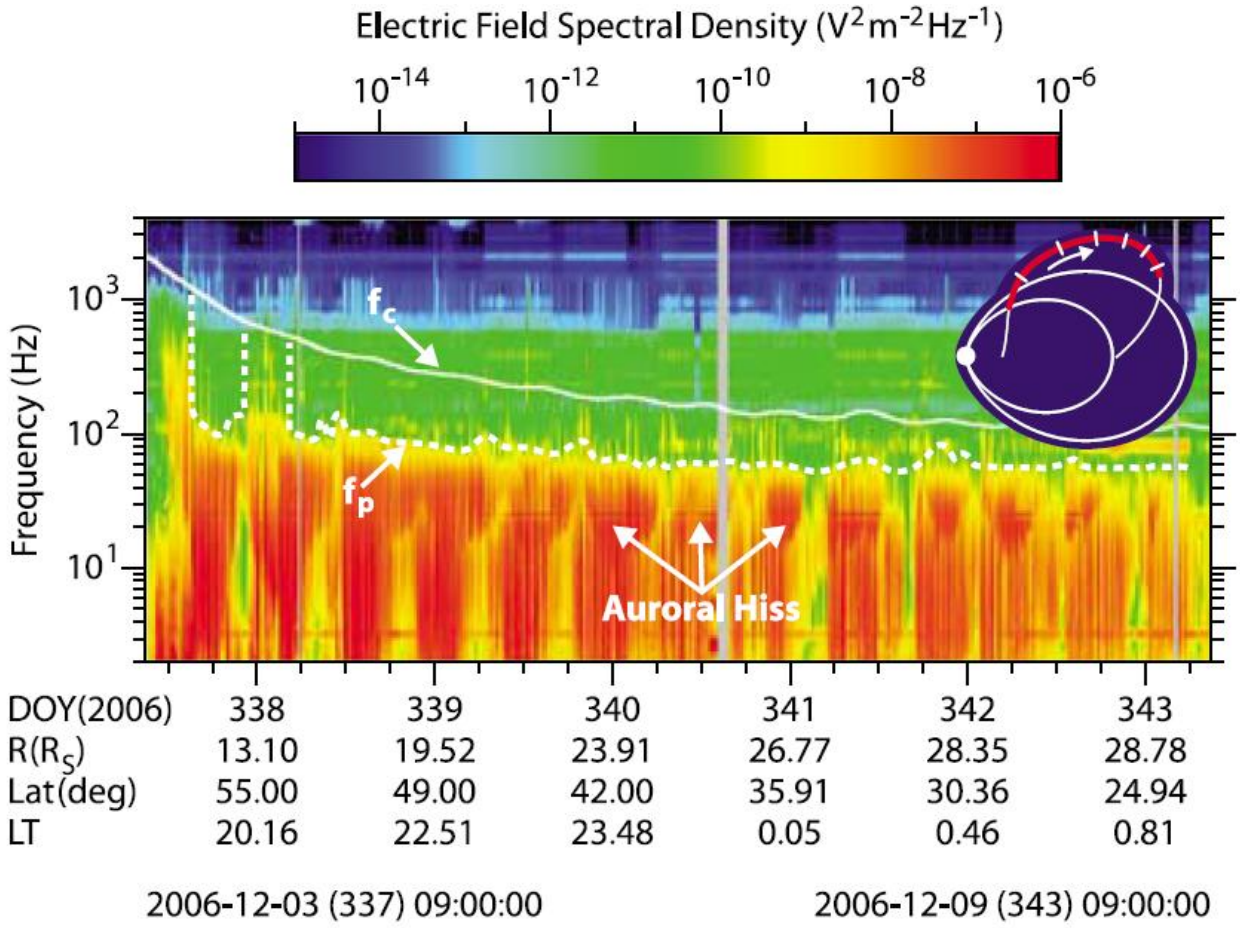

Figure 16 – Seven days of Cassini data, revealing a periodicity in auroral hiss emissions. The observed modulation is on the order of the rotational period of Saturn. The electron cyclotron frequency (f_c) and the electron plasma frequency (f_p) are indicated throughout the orbit.

order of the rotation period of Saturn, between 10.6 and 10.8 hours. The exact planetary rotation period is difficult to determine, as the radio periodicities may follow the rotating plasma and not the core of the gas giant itself. In any case, at first glance, the modulation of auroral hiss appears to correlate well with the periodicity of the Saturn Kilometric Radiation (SKR), which appears at higher frequencies of the displayed data. The periodicity of the SKR has been studied closely in recent years, and it has been used to calculate a rotation rate and longitude system for Saturn, the most recent version of which is known as the SLS-3 longitude system [*Kurth et al.*, 2008].

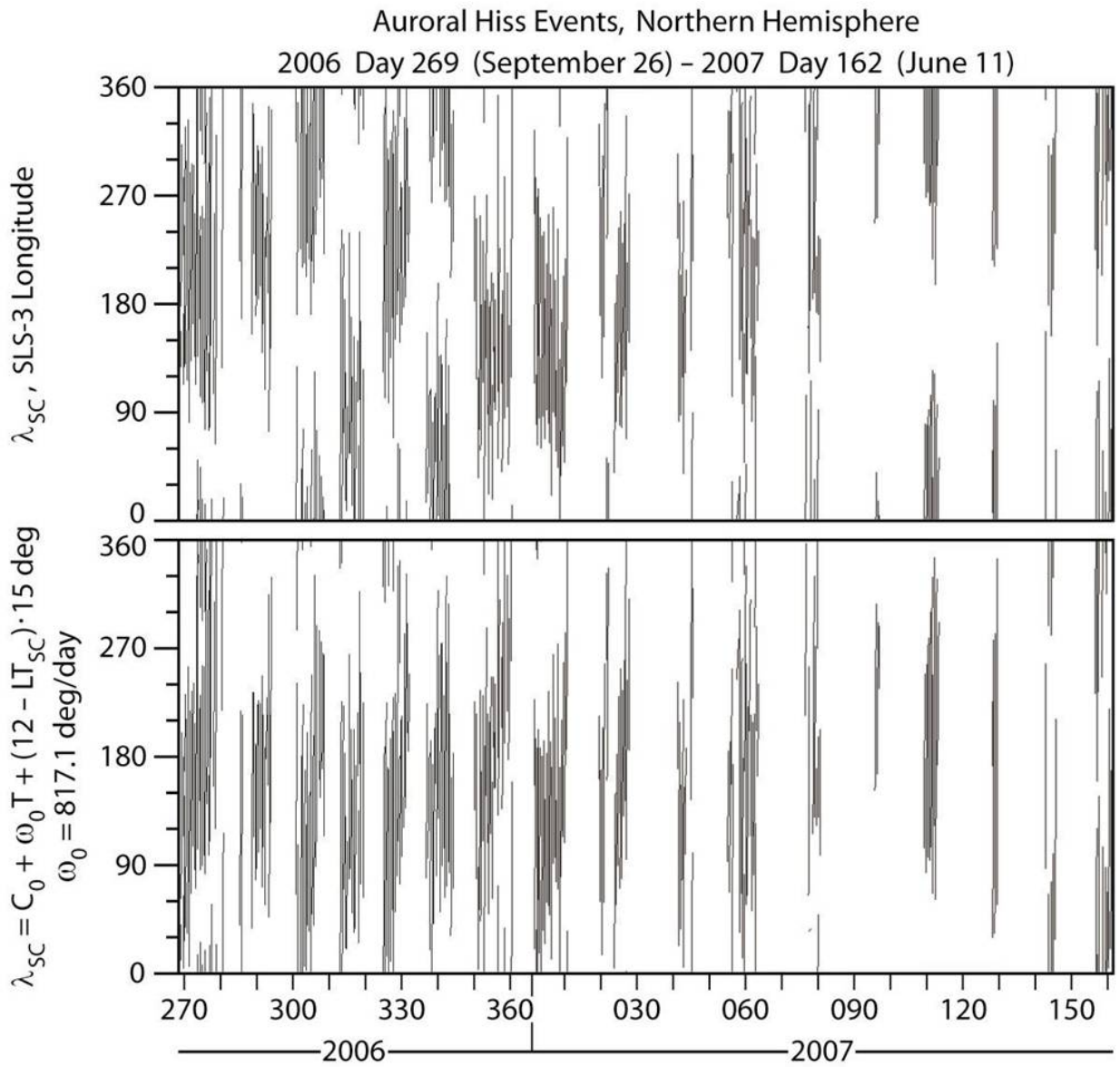

Figure 17 – Periodicity of the auroral hiss emission, using two different longitude systems. The auroral hiss modulation does not correlate well with the SLS-3 system that maps SKR emissions (top panel), but organizes well to a rotating beam model at a faster rotation rate.

One perhaps surprising observation was that the auroral hiss modulations did not follow the same periodicity as the SLS-3 system. Figure 17 shows a pair of longitude versus time plots, using the SLS-3 longitude system to calculate the corresponding longitudes of the emission. The data were taken from the roughly nine-month period where Cassini was first in higher inclination

orbits. When auroral hiss detections are plotted using the SLS-3 longitude system, as shown in the top panel, the observations do not organize well.

In order to determine a more accurate periodicity from the auroral hiss emission, the data were reorganized using a generic rotating beam source model, as shown in the lower panel of Figure 17. In this model, there are only two free parameters, the first being a constant representing the initial longitude at time T=0, and the second the frequency of rotation of the emission (ω_0). The frequency was adjusted incrementally, and at each step the quality of the organization of the data was determined. The frequency which best organized the data was 817.1 degrees per day, corresponding to just less than 10.6 hours for a planetary rotation rate, faster than the rate found for the SKR using the SLS-3 model.

The fact that auroral hiss can be fit by a rotating beam model, however, is not sufficient evidence to conclude that this emission is a rotating beam source. It is clear that this model provides a good fit to the data, but it may not be the only model, or even the best model, that neatly organizes the emission data. One other model, a clock-like source of emission, would also make sense physically. To test which one provides a better fit to the data, the rotational modulation spectrums for each model were computed. To do this, as performed by *Gurnett et al.* [2009a, 2009b], the normalized auroral hiss intensities were sorted and averaged in one degree bins in longitude for a series of assumed rotation rates, ω. For each ω, the resulting averages were fit to a sinusoidal function of longitude, which yielded the amplitude and phase of the modulation. To determine whether it was more like a clock-like source or a rotating beam, two longitudes were used. For the clock-like model, the longitude of the Sun ($\lambda_{Sun} = \omega T$) was used, where T is the Universal Time (UT) of the spacecraft, while the rotating beam model used the spacecraft longitude [$\lambda_{SC} = \omega T + (12 - LT_{SC}) \times 15°$], where LT_{SC} is the spacecraft local time.

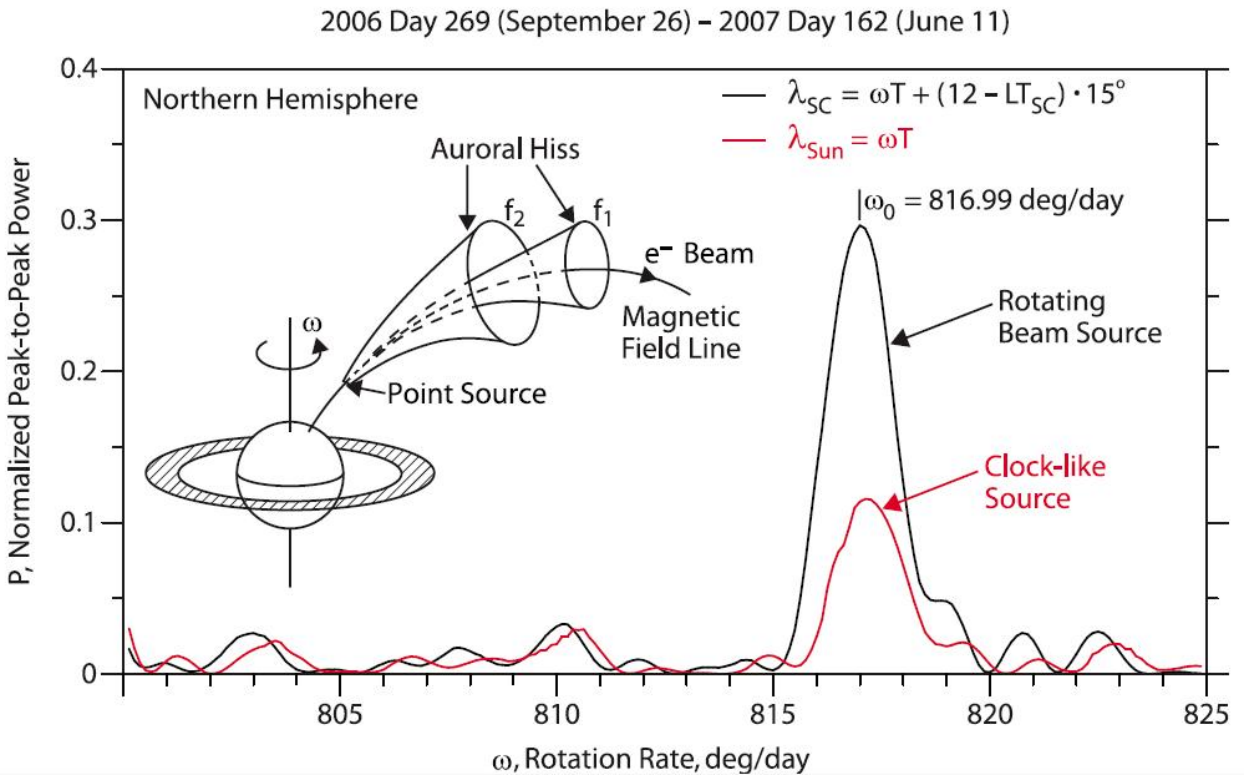

Figure 18 – Modulation spectrum for two source models. The rotating beam source shows a stronger correlation for auroral hiss. Incompleteness and non-uniformity in the local times observed by Cassini, due to its orbital path, account for most of the residual peak for the clock-like modulation model.

The resulting modulation spectrum is shown in Figure 18, which plots the best fit peak-to-peak amplitude as a function of the frequency for all northern hemisphere events during Cassini's first tour of the high-latitude regions at Saturn. Two plots are shown, one with a black line for the rotating beam model, and the other a red line for the clock-like source. It is worth noting that, while both models have their peak at 817.0 ± 0.9 degrees per day, the rotating beam model has a very sharp peak at a significantly larger amplitude, implying a the source is almost certainly a rotating beam. In fact, the existing peak in the clocklike model is likely only due to a selection effect, as the sampling of data in this period is not uniform in local time.

One of the more puzzling rotation-related finds at Saturn is the discovery that multiple periodicities exist even within common radiation elements. It is now known that the SKR modulation consists of two distinct periods [*Kurth et al.*, 2008]. This was recently expanded on by *Gurnett et al.* [2009a], who reported that these two components were actually the product of a north–south difference in the rotational modulation rate of Saturn Kilometric Radiation (SKR). The SKR emanating from the northern auroral region was determined to have a periodicity of 10.6 hours, while the corresponding emission from the southern hemisphere modulated instead at 10.8 hours. Furthermore, these periods were not constant. As Cassini approached the Kronian equinox, the two periods appeared to be approaching each other.

Later that year, *Gurnett et al.* [2009b] sought to learn whether auroral hiss possessed the same north-south asymmetry. In order to determine the modulation period of auroral hiss to accuracy comparable with the SKR measurements, i.e., better than 1%, the period must be averaged over long intervals of 100 days or more. Since the orbital period of Cassini is typically between 10 and 30 days, this requires averaging over many orbits. To add to the difficulty, since Cassini has only been in the high latitude regions during two segments of its mission at Saturn, there is a very limited range of times where this periodicity can be determined to good precision.

Unfortunately, since Cassini made only brief excursions to the high-latitude regions in the southern hemisphere during the first period of high-latitude orbits, it is not possible to measure an accurate modulation rate during this segment. A much better opportunity to obtain simultaneous measurements of the rotation rate of the auroral hiss in both hemispheres occurred during the second interval of high latitude passes. During this interval the spacecraft orbit was such that good auroral hiss observations, with well-defined rotational modulations in both the northern and southern hemispheres, could be made from about Day 358, 2008, to Day 167, 2009.

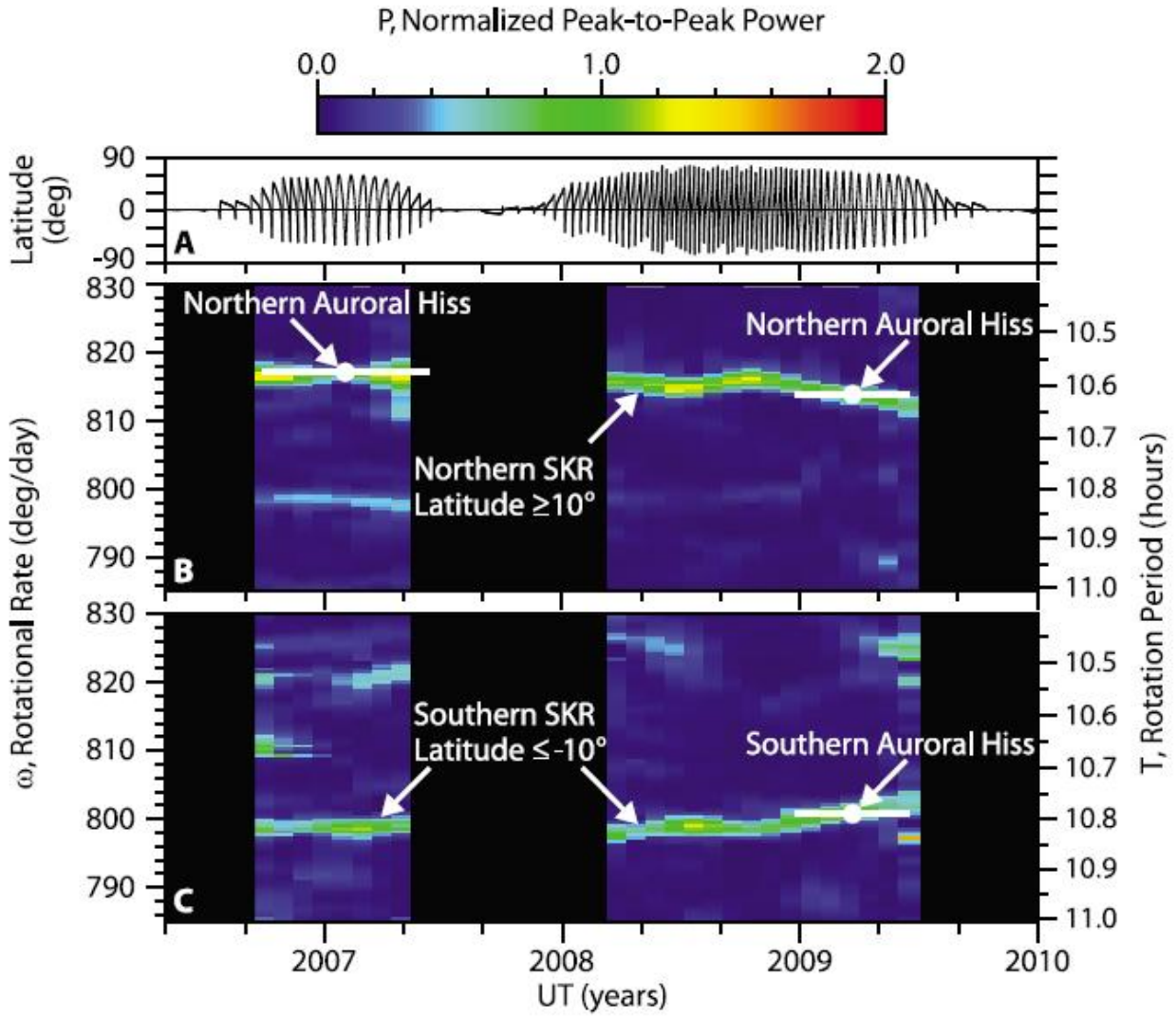

Figure 19 – Rotational modulation of SKR and auroral hiss, revealing a north-south asymmetry in the rotation rates of these emissions. The horizontal bars on the auroral hiss points indicate the range over which the data were average to obtain the modulation rate.

Using the same spectrum analysis procedure shown in Figure 17, the rotation rates of the auroral hiss in the northern and southern hemispheres during this interval were found to be 813.9 ± 0.8 deg/day and 800.7 ± 0.9 deg/day, respectively. These rotation rates are shown in Figure 19 by the white dots at the center of the interval, which is day 79, 2009. The horizontal white lines indicate the duration of the analysis intervals and the vertical size of the dots are comparable to

the uncertainties in the rotation rates. As can be seen, the auroral hiss rotation rates in the northern and southern hemispheres match almost exactly the SKR rotational modulation rates in those hemispheres. The SKR rotation rates in the northern and southern hemispheres averaged over this same time interval were 813.8 ± 0.9 deg/day and 801.0 ± 1.1 deg/day, respectively. This asymmetry and its correlation with the asymmetry of the SKR modulation likely have important implications for how the planetary rotation is coupled to the magnetospheric plasma.

It is interesting to note that even though they occur at almost the same rate, the rotational modulation processes involved in the auroral hiss and the SKR are fundamentally different. The SKR modulation is known to be clock-like, with the radiation blinking on and off from a high-latitude source in the late local morning [*Desch and Kaiser*, 1981], whereas auroral hiss modulation has now been shown to be caused by a rotating beam. Also, the radio emission mechanisms are quite different. SKR is believed to be generated via the cyclotron maser mechanism [*Wu and Lee*, 1979] by an anisotropic distribution of electrons accelerated downward along the magnetic field lines by parallel electric fields, whereas auroral hiss detected by Cassini is believed to be generated by an electron beam moving upward along the magnetic field lines.

In addition to this long-scale periodicity, the low-frequency region of RPWS electric sensor data also reveals a short-term variation on the order of one hour. The periodicity appears as an enhancement in the intensity, and is a common feature, found in a majority of the auroral hiss events detected at Saturn. An example of this is shown in Figure 20, from *Mitchell et al.* [2009], where enhancements in the emission intensity are clearly visible roughly every hour roughly over a four-hour period.

Analysis of particle data has revealed that these bursts are accompanied by increases in the density of both ions and electrons, associated with the presence of upward-propagating ion

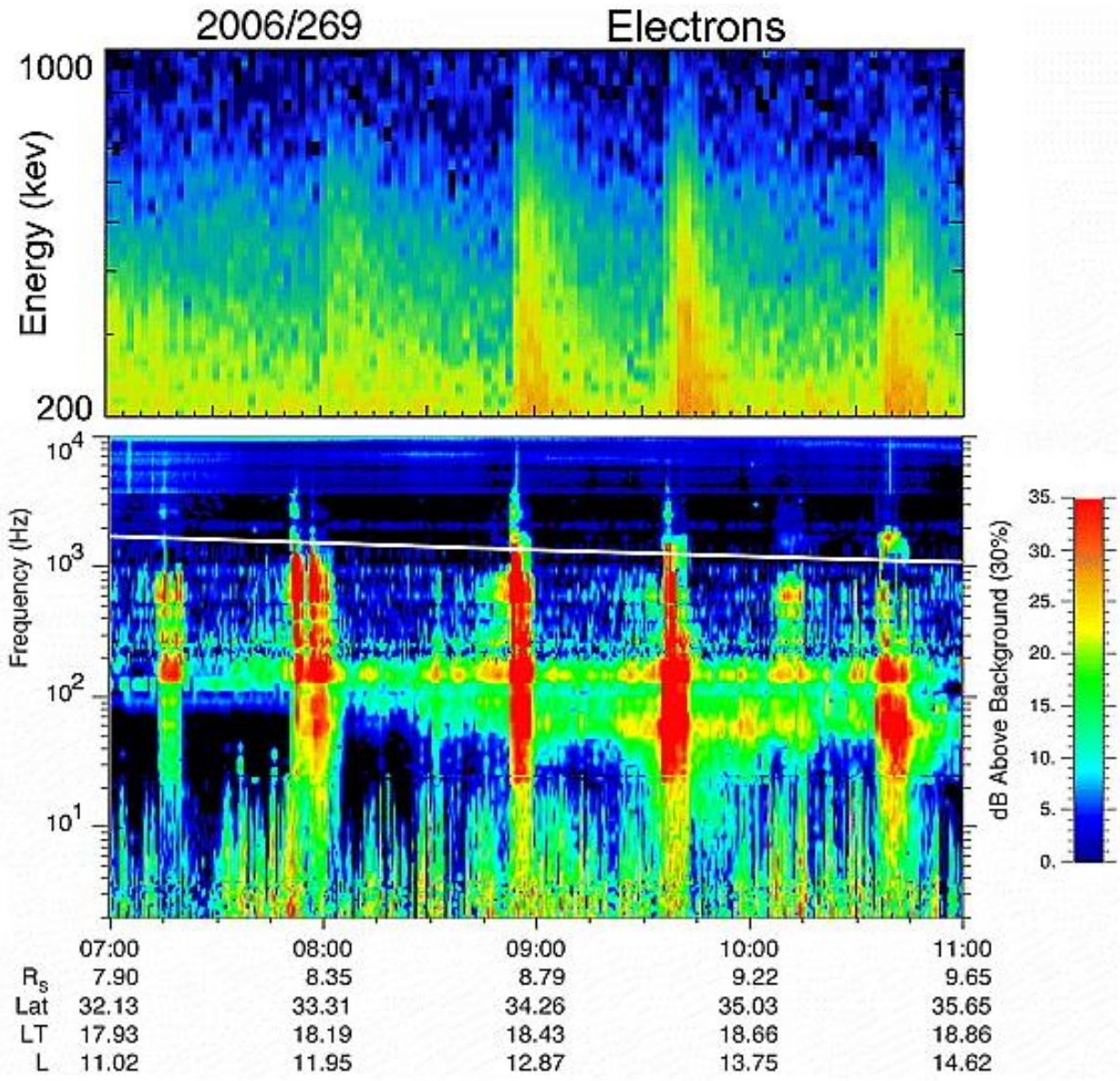

Figure 20 – Periodic intensity enhancements in the frequency range where auroral hiss is commonly observed, as reported by *Mitchell et al.* [2009]. Bursts of ions and electrons are found to coincide with these events.

beams and electron enhancements. These electrons are believed to be from electron beams that have been backscattered by field irregularities farther out the flux tube, [*Mitchell et al.*, 2009]. All ion events have been observed by the MIMI instrument to be upgoing, while electron enhancements have been either upgoing or bidirectional, but never exclusively downgoing.

None of these particle events have ever been detected by Cassini in regions where L < 9, either as a result of the higher isotropic background density or simply the lack of beams entirely in these regions.

During these pulses, the magnetic field angles exhibit abrupt changes by about 2-3 degrees, and then return to their previous values. This behavior is consistent with the repeated passage of field-aligned current structures. Although the highest burst intensities appear in a frequency range consistent with the whistler mode, these events can extend to frequencies above the cyclotron frequency, as in Figure 20, which is outside the boundary of allowed whistler-mode propagation. Coupled with the lack of a magnetic component above the cyclotron frequency, this result suggests an electrostatic mode from the components above this frequency. Overall, given the fairly steady periodicity of these events, it is believed that these regular bursts are caused by flux tube interchange relatively close to the auroral zone [*Mitchell et al.,* 2009].

4.4 Field-Aligned Currents

Although auroral hiss is not caused by steady currents, field-aligned currents are also expected to be present in these regions due to the physical mechanisms involved in the generation of electron beams. Since auroral hiss is generated by field-aligned electron beams, and therefore at least initially propagates such that it is centered about the magnetic field line, theory suggests that these currents would be observed consistently in correlation with the radio emissions. Since these currents are carried by the electron beams that generate the emission, their presence would be an indicator of the existence and location of these beams that are producing the auroral hiss. However, unlike the data presented to this point, these are unable to be detected directly by the RPWS instrument. This instead requires measurements from the

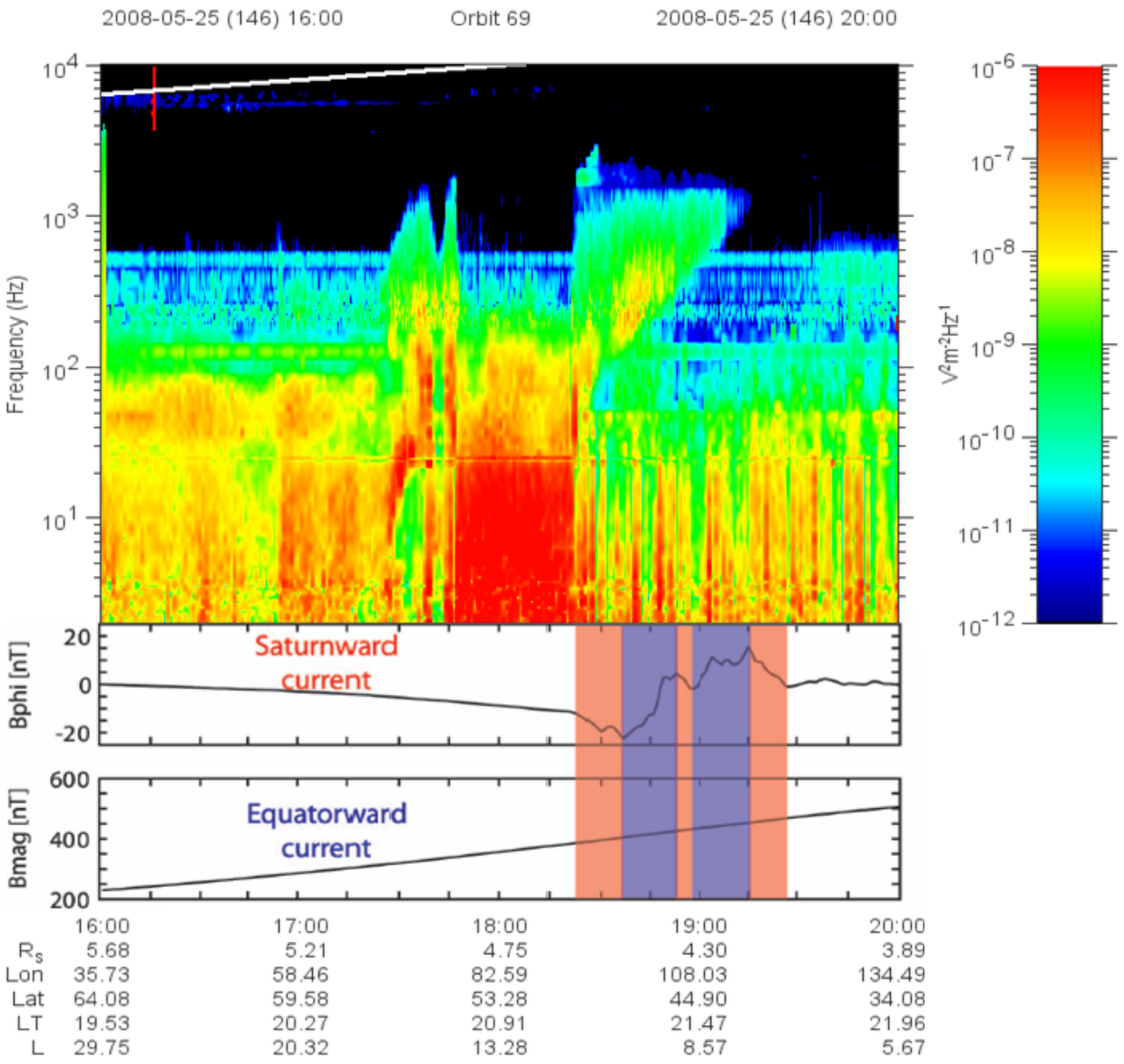

Figure 21 – Field-aligned currents associated with auroral hiss radio emission. The currents always occur in conjunction with the ledge-like step on the equatorward side of the emission, and are dominated by an upgoing current situated between two weaker downgoing currents.

magnetometer (MAG), which can detect variations in the magnetic field. Since these currents would be propagating along the field lines, variations in the B_φ component will be the most significant observations, as a current flowing parallel to the direction of propagation of the radio emission would induce a magnetic field component in that direction.

Figure 21 displays an example of how these field-aligned currents correlate with the radio emission. This example is characteristic for the cases we have studied in this research. It is very common to see these current structures in conjunction with the auroral hiss emission, to the point where it is more curious when they are not observed. It initially came as a bit of a surprise, however, that these current structures are not observed at the center of the auroral hiss, but rather at the equatorward edge. This result begged other questions, most importantly the reason for this deviation from the standard model of auroral hiss emissions.

A similar result is observed when looking at a wider time frame and at a different trajectory, as illustrated in Figure 22. Here, Cassini is in a highly inclined orbit, and this snapshot is centered on Cassini's crossing from the northern hemisphere through the ring plane and into the southern hemisphere. On each side of the spectrogram shown in the top image, we observe strong auroral hiss radio emission once sufficient latitude is reached. In the lower figure, spikes in B_φ are observed, indicating the presence of field-aligned current structures as Cassini passes through these regions. Again, however, these spikes are observed to be on the equatorward edge of the emission, not in the center, implying these currents are not likely associated with the electron beams that generate the observed emission.

As noted previously, these currents are now known to mark the boundary of a higher density region at Saturn that is bounded roughly at an L-shell of L ~ 12-15, similar to the plasmapause at Earth. This magnetically-confined region of low-energy plasma has been routinely observed to be bounded on its exterior by the tri-current system shown in Figure 22. In this system, a very strong upgoing field-aligned current is flanked on both the inside and outside by a weaker downgoing field-aligned current structure, all of which surround this region of high-density plasma. Coinciding with the boundary marked by these currents, the density drops by at

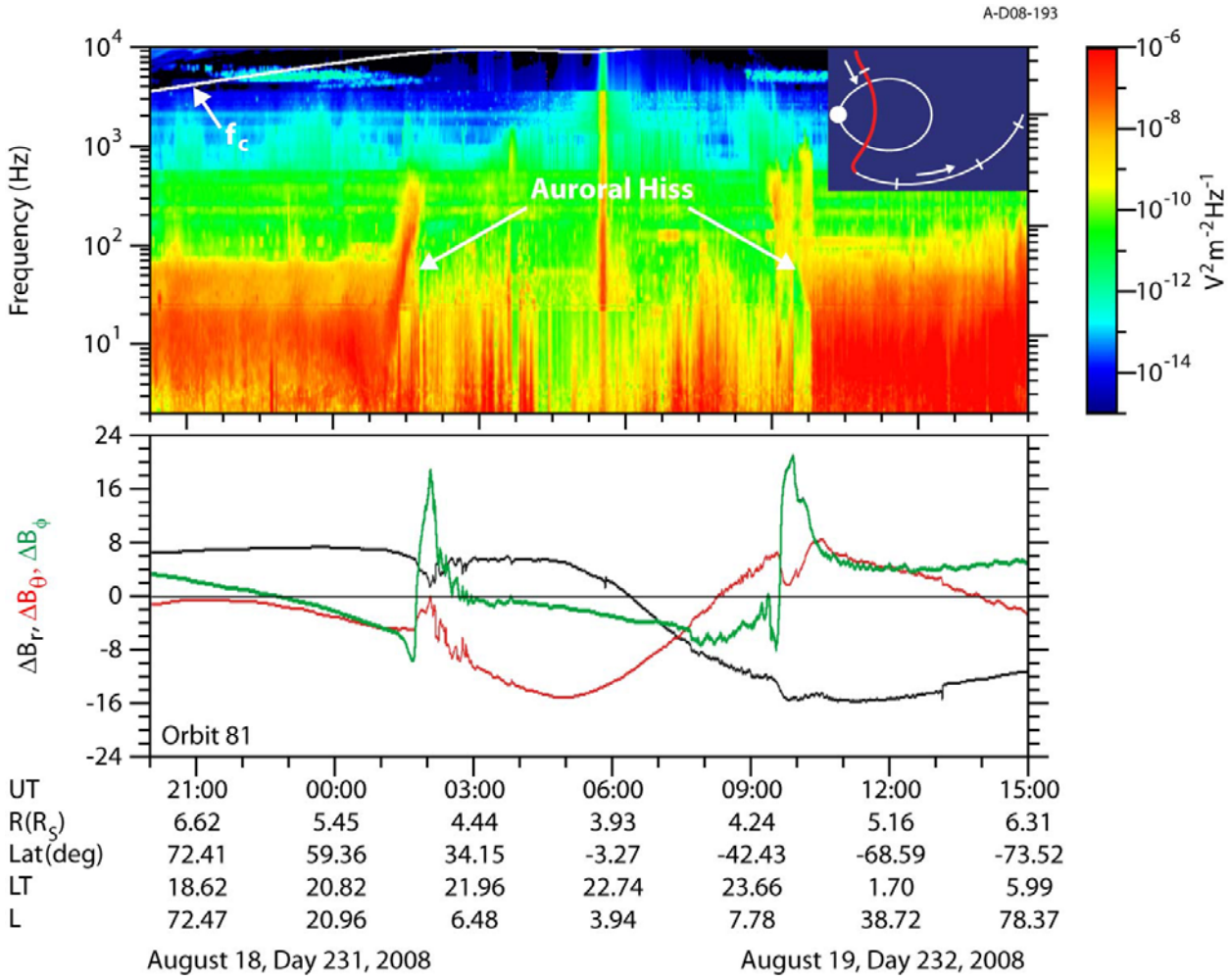

Figure 22 – Dual-hemisphere comparison of RPWS and MAG data. The field-aligned current structures, dominated by an upgoing current structure, mark a boundary between a high-density region at low L-shells and a low-density region in the auroral zones.

least an order of magnitude, creating a plasmapause-like boundary that separates the plasmasphere from the lower-density auroral regions, which also contain a much weaker distributed return current to complete the current loop. This system is detailed in Figure 23.

Finally, it is worth considering how this current system relates to the generation of the two major magnetospheric processes discussed here, namely the SKR and auroral hiss. Since the SKR is known to be most strongly generated in the late local morning side of the magnetosphere, it is plausible that the radiation switches on as some rotating plasma feature is carried through

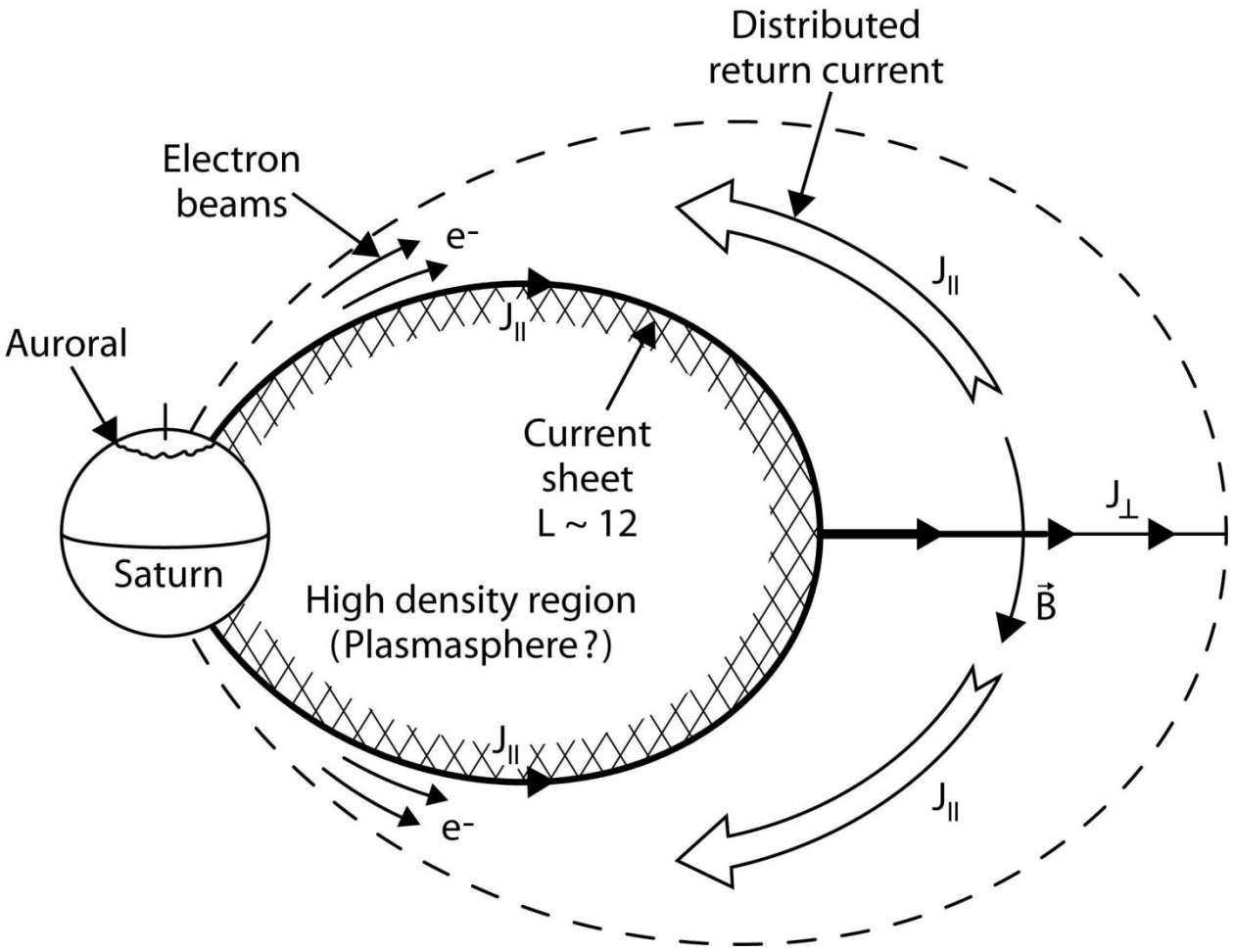

Figure 23 – A proposed model for the Saturn current system, including a high-density plasmasphere region at low L-shell values, bounded on its exterior by a tri-current region dominated by an upgoing field-aligned current.

this region, perhaps due to enhanced reconnection or some other physical process that arises as the plasma interacts with the morning-side magnetopause.

With this general picture in mind, it is interesting to investigate the phase difference between the auroral hiss and the SKR modulations. *Gurnett et al.* [2009b] showed for the second time interval where Cassini is in high-latitude orbits that the auroral hiss source is rotating through the local afternoon side of the magnetosphere at the time that the SKR reaches maximum intensity in the late local morning side of the magnetosphere. Since the auroral hiss is

believed to be generated by up-going electrons accelerated by parallel electric fields and the SKR is generated by comparably accelerated downgoing electrons, these results suggest that the currents carried by these electrons may be part of a large-scale rotating current system.

One additional explanation of this type was proposed by *Southwood and Kivelson* [2007]. In this system the current flows down the high-latitude magnetic field lines on one side of the magnetosphere, horizontally through the ionosphere, and then upward along the high-latitude magnetic field lines on the other side of the magnetosphere. If such a current system is involved in the generation of the auroral hiss and SKR, then the currents would have to consist of two components that rotate at different rates in the two hemispheres, which at the present time is quite difficult to comprehend.

CHAPTER 5

ELECTRON BEAMS AND GROWTH RATE ANALYSIS

5.1 Observations

The final key aspect of auroral hiss emissions is particle beams, particularly electron beams. At Earth, both through theory and then experimental testing, auroral hiss is now believed to be generated by an electron beam-plasma instability caused by the motion of electron beams through the magnetosphere. As a result, in order to explain auroral hiss emission at Saturn, it is necessary to identify electron beams that appear in conjunction with the radio emissions, and then determine if these beams are sufficient in velocity and energy to produce the observed radiation in the RPWS spectrograms.

In order to locate these electron beams, we turn to the CAPS investigation, specifically the electron spectrometer (ELS). Figure 24 shows an example of ELS data, which was chosen specifically for the appearance of an electron beam. These data were integrated over two minutes to provide good pitch-angle coverage, and then binned in pitch-angle increments of ten degrees. The beam can be clearly identified along the horizontal axis on the left side of the image. As one would expect, this beam appears in conjunction with intense whistler-mode emission found in the RPWS spectrograms.

One curious observation that has come out of the particle instrumentation is that correlation exists not only in the electron beams, but also the ion beams. Figure 25 shows an RPWS spectrogram, with the addition of red bars along the horizontal axis to represent the time periods where ion beams have been observed by the MIMI instrument. This remarkably good correlation came as a bit of a surprise initially, as ion beams are not believed to play any role in

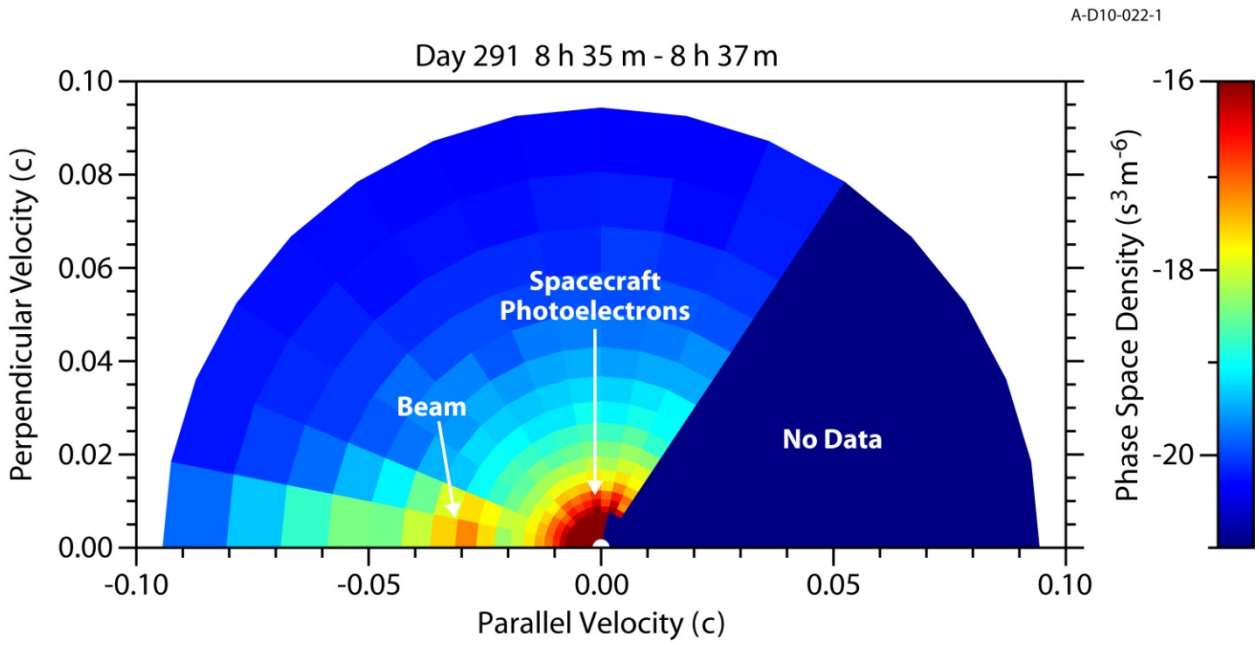

Figure 24 – An electron beam observed with the ELS instrument. The upward-propagating beam is seen along the horizontal axis, closely aligned with the magnetic field. ELS measurements were averaged over two minutes to provide good pitch-angle coverage.

the generation or propagation of auroral hiss. However, combining this discovery with reports of downward propagating ion events from the FAST spacecraft, as described in Chapter 2.3, suggests that the detection of ion beams should perhaps be an expected result. Regardless of whether this correlation is coincidence or not, the fact that these detections again appear on the equatorward side of the radio emission suggests that these beams are likely associated with the field-aligned current structures at the boundary of the plasmasphere.

On 17 October 2008, the Cassini spacecraft was in a high-latitude pass at very low altitudes. During this pass, at 8:35 UT, ELS detected an intense, upward-moving, field-aligned electron beam at an energy of about 200 eV, shown in Figure 24. The beam can be seen as the enhancement in the phase-space density along the negative horizontal axis. The ELS data in this figure have been integrated over two minutes to provide good pitch-angle coverage. This

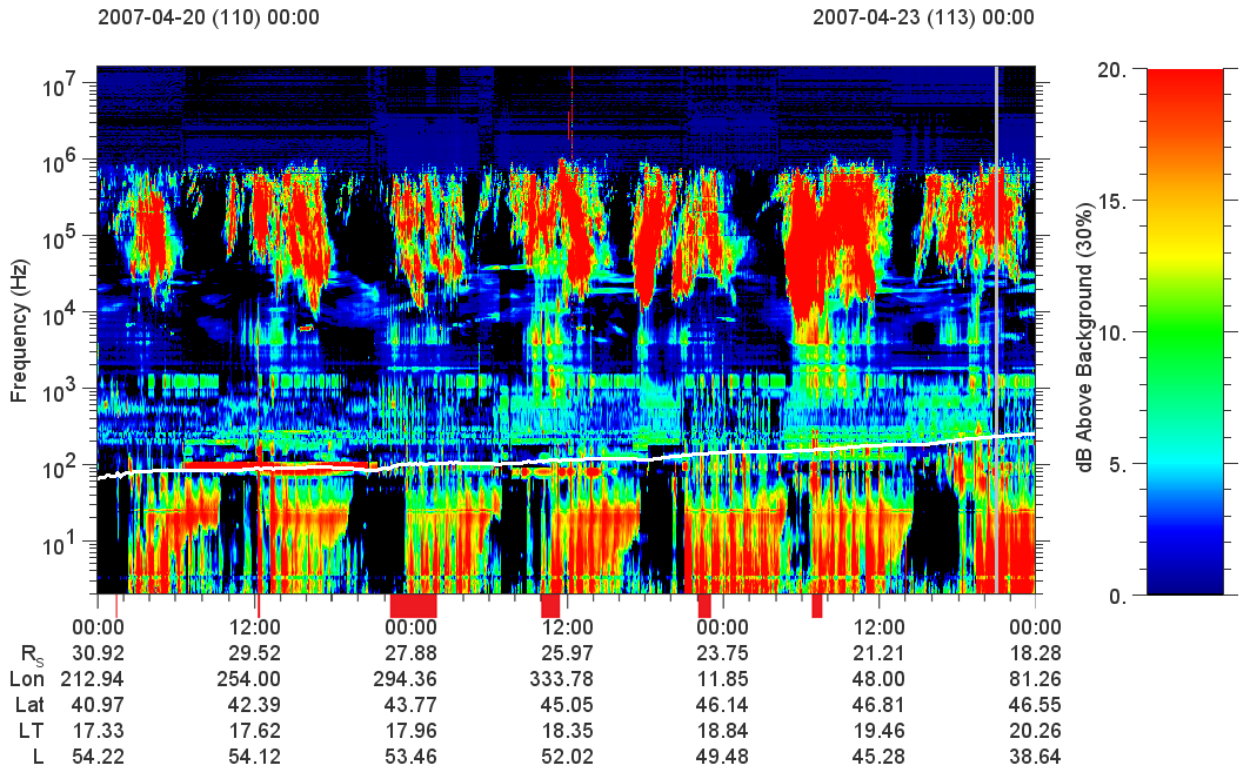

Figure 25 – The correlation of ion beams with the auroral hiss emission. Red bars on the horizontal axis indicate the detection of ion beams. Although not required for the generation of auroral hiss, the presence of ion beams has been observed at both Earth and Saturn in correlation with this emission.

upward propagating electron beam is exactly the type of velocity distribution expected for the generation of auroral hiss via a beam-plasma instability [*Maggs*, 1976].

At the same time as the beam, strong broadband low-frequency emissions, likely in the whistler-mode, were also observed by RPWS, as shown in Figure 26. This emission in the region of the electron beam does not display the typical funnel-shaped emission of auroral hiss, instead appearing more burst-like in nature. However, this is not unlike terrestrial auroral hiss, which often displays similar burst-like electrostatic noise in the source region [*Lonnqvist et al.*, 1993], suggesting the possibility Cassini may have been in or very near the source region of the auroral hiss when making this observation.

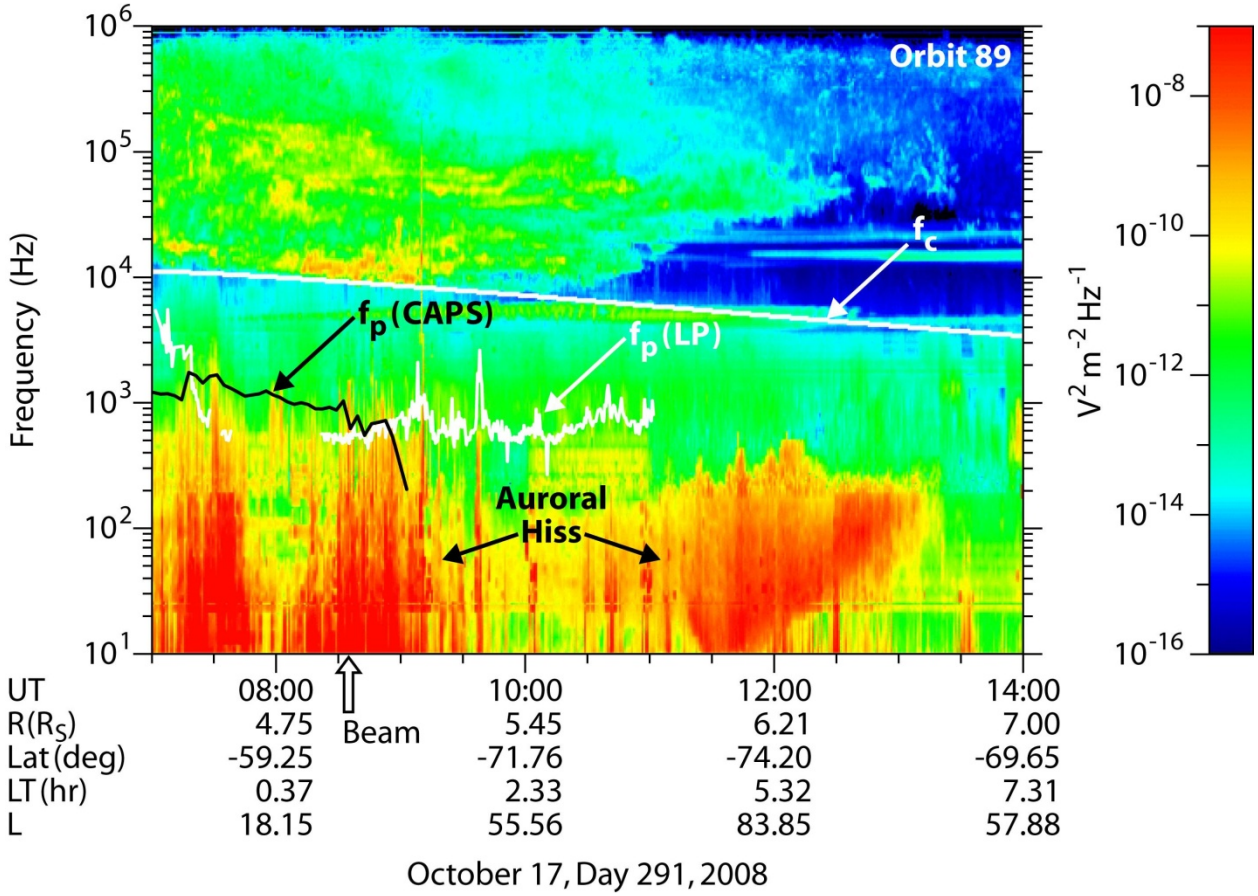

Figure 26 – RPWS spectrogram from October 17, 2008. Burst-like auroral hiss appears in conjunction with the detection of an electron beam, while a funnel-shaped region appears a few hours later. Also indicated are the plasma frequencies derived from the CAPS instrument and Langmuir Probe, and also the cyclotron frequency. The location of the 8:35 UT beam is marked on the horizontal axis.

The top two panels of Figure 27 show the power spectra of the magnetic and electric components of the plasma wave, respectively. Since Poynting vector analysis requires the usage of both the electric and magnetic components, both are necessary to be present to determine the direction of propagation of an observed radio emission. In the case of the emission observed coincidentally with the beam around 8:35 UT, the very weak magnetic signature made it impossible to conclude which direction the wave was propagating. However, the subsequent V-shaped auroral hiss funnels observed at roughly 12:00 UT and at around 17:00 UT have large

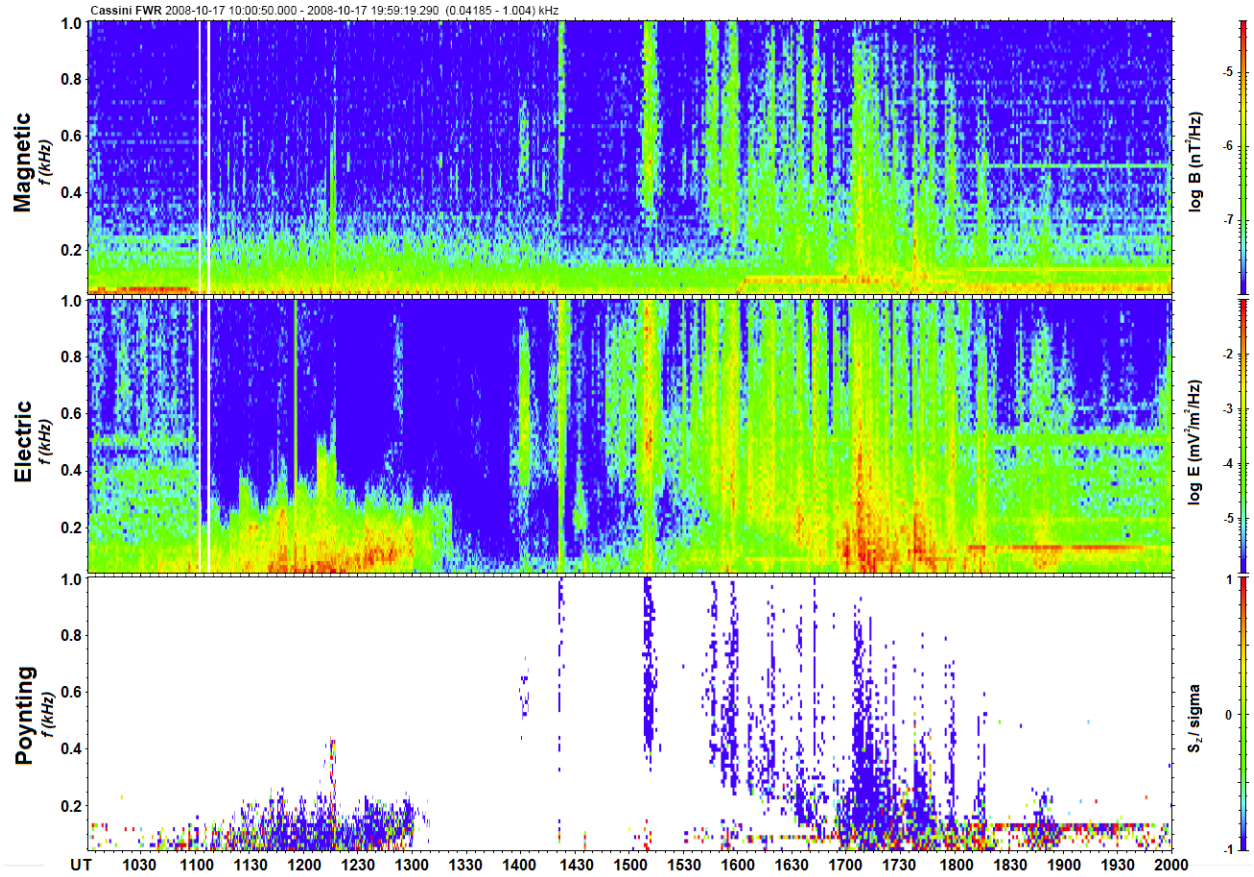

Figure 27 – Propagation analysis of two funnel-shaped features on October 17, 2008. The top panel shows the magnetic spectrum, while the middle displays the electric component. The Poynting analysis displayed in the bottom panel shows these waves are propagating anti-parallel to the magnetic field, which in Saturn's southern hemisphere implies upward propagation.

enough magnetic components to allow for this determination to be made. In both cases, as shown in the third panel of Figure 27, the emission is propagating anti-parallel to the magnetic field of Saturn. Since we are in the southern hemisphere, where the planet's magnetic field is directed downward toward the planet, the emission is propagating upward.

5.2 Analytical Growth Rate Analysis

While showing correlation between all the different components of auroral hiss emission is crucial, it is not sufficient for drawing conclusions about their connection. It is important to

remember that correlation does not necessarily imply causation. In order to truly demonstrate that any detected electron beams are the source of this radiation, a growth rate analysis must be performed. It must be shown that the observed electron beams possess the correct distribution of energies and velocities to produce the observed radio emission, which can be done by solving the dispersion relation to obtain the growth rate. Calculations using model beams have been performed by *Maggs* [1976], but the first calculations using experimental data at Saturn are presented here, as described by *Kopf et al.* [2010].

For plasmas, it is often cumbersome to calculate the growth rate. In practice, the dispersion relation can only be solved for a few select cases, which generally appear only as idealized approximations to real physical systems. Even the process of obtaining the dispersion relation itself can often be an ambitious undertaking. Fortunately, however, the foundation for the computation in this case had already been completed [*Kennel and Wong*, 1967]. Without approximation, the growth rate was computed for plasma waves in any branch of the dispersion relation and propagating at nearly all angles to the magnetic field, which was published as Equation 9 in *Kennel and Wong*:

$$\frac{\gamma_k}{\omega_k} = sign\left(\frac{\omega_k}{k_{\|}}\right)\sum_{\pm}\sum_{m}\left(\frac{\omega_p}{\omega^2}\right)\frac{\pi}{16}\int_0^{\infty} v_{\perp}^2 dv_{\perp}\int_0^{\infty} dv_{\|}\delta\left(v_{\|} - \frac{\omega_k + m\Omega_{\pm}}{k_{\|}}\right)\frac{\theta_m^{\pm} G_k^{\pm}}{W\left(k,\omega_k\right)} \qquad (1)$$

Here, W(k,ω) is the energy density of the wave, where k is wave number and ω is the frequency. Also, $\Omega_{\pm}$ is the cyclotron frequency for each species, $G_k^{\pm}$ is the species-dependent reduced one-dimensional distribution function, and $\theta_m^{\pm}$ is a weighting function. A cylindrical coordinate system centered on the static magnetic field direction was used, and the k-space angle ψ is defined such that $\sin\psi = k_y / k_{\perp}$. The weighting function, $\theta_m^{\pm}$, is defined to be

$$\theta_m^{\pm} = \left| J_{m\pm1}\varepsilon_l e^{-i\psi} + J_{m\mp1}\varepsilon_r e^{i\psi} \pm 2^{1/2}\frac{v_{||}}{v_{\perp}} J_m \varepsilon_{||} \right|^2 \quad (2)$$

where ε_l and ε_r represent left-handed and right-handed circular electric field polarizations about the magnetic field direction, respectively, and $\varepsilon_{||}$ is the linear polarization along the field.

This method, however, is clearly still very complex and cumbersome to work with. The multiple coordinate systems and cylindrical geometry necessary for the calculation demand a very abstract approach, and the prospect of utilizing these multiple systems simultaneously, along with a series of Bessel functions, to calculate a complex weighting factor should give any scientist pause. This result would be very difficult to interpret and to check for accuracy. Ideally, a simpler method, making use of a single coordinate system, would be more practical to work with. Even with minor approximations, its results should be far easier to work with, interpret, and check. Fortunately, such a method had been employed about fifteen years ago that, although originally designed for a different purpose, had direct applications to this computation.

To calculate the growth rate analytically, I instead followed the model used by *Morgan et al.* [1994]. The starting point comes from *Kennel* [1966], who derived the linear growth rate for waves propagating in a collisionless, homogeneous, magnetized plasma, assuming resonance velocities well above the thermal velocity of the distribution function, and a growth rate that is small compared to the wave frequency. His formula is lengthy and therefore is not repeated here. However, a few simple assumptions reduce it to a more manageable form. First, we assume that the waves are propagating near the resonance cone, which is expected for auroral hiss [*Mosier and Gurnett*, 1969]. Second, we assume that ions play a negligible role in the wave propagation. Kennel's equation then reduces to

$$\gamma \frac{\partial D^{(0)}}{\partial \omega} = \frac{8\pi^2 n^4 \omega_p^2}{k^2 n_0 \left|\cos(\theta)\right|} \sum_m \int_0^\infty dv_\perp J_m^2 \left(\frac{k_\perp v_\perp}{\omega_c} \right) \left[\frac{m\omega_c}{k} \frac{\partial f}{\partial v_\perp} + v_\perp \cos(\theta) \frac{\partial f}{\partial v_{||}} \right], \qquad (3)$$

where γ is the growth rate, $D^{(0)}$ is the cold plasma determinant defined by *Stix* [1962], n is the index of refraction, ω_p is the plasma frequency, k is the wave number, n_0 is the electron density, θ is the wave normal angle, ω_c is the electron cyclotron frequency, *f* is the phase-space distribution function, and J_m is a Bessel function of order m. The parallel component of the velocity, $v_{||}$, is evaluated at the resonance velocity, $\omega/k_{||}$.

From Figure 26, we observe that at 8:35 UT, the electron cyclotron frequency, f_c (where $f_c = \omega_c/2\pi$), as calculated from magnetometer measurements, is about 10 kHz. Measurements of the electron density from the Langmuir Probe and the CAPS instrument show that the electron plasma frequency, f_p, is much lower, roughly 500 Hz. Thus, we now make the approximation that $f_c^2 >> f_p^2 > f^2$, where f is the emission frequency. Although not true for all times at Saturn, this holds in the cases presented in this dissertation, and greatly simplifies Equation (3).

We further recognize that we only need the m=0 term in the Bessel Function series. Since the Bessel functions where m is nonzero scale like the argument to the m-power, the J_0 term will dominate when the argument is small. By definition, the ratio J_1^2/J_0^2 will be approximately equal to the square of the Bessel Function argument. For the observed beam velocities, it can be easily shown that this argument is small. Since these beams are roughly field-aligned, the perpendicular component of the velocity is very minimal, on the order of v/10, where v is the beam velocity. Furthermore, because of the resonance cone propagation, the k-vector is almost entirely perpendicular. Substituting this information into the Bessel Function argument, it can easily be shown that the argument scales like $(vn/c)*(f/f_c)$, where n is the index

of refraction. Since v is only a small fraction of c, n is of order unity, and the characteristic frequency, the frequency of the strongest emissions, is two orders of magnitude less than the cyclotron frequency for the cases evaluated in this study, the argument will always be very small.

As a result, the terms where m is nonzero become negligible compared to the m=0 term when convolved with the observed distribution function. This eliminates the first term of the integral, leaving only the $\partial f/\partial v_{||}$ term. Also, since the argument of the Bessel function can be shown to be small, we can approximate J_0^2 as 1, since the second term in the expansion will scale like the square of the small argument. Cancelling common terms yields

$$\gamma = \frac{2\pi\omega_p^2\omega}{k^2}\frac{\partial}{\partial v_{||}}\left[\frac{1}{n_0}\int_0^\infty dv_\perp 2\pi v_\perp f\left(v_\perp, v_{||}\right)\right]. \tag{4}$$

We now define the bracketed part of Equation 4 to be the reduced distribution function,

$$F(v_{||}) = \frac{1}{n_0}\int_0^\infty dv_\perp 2\pi v_\perp f(v_\perp, v_{||}). \tag{5}$$

Inserting this into Equation (4), along with the Landau resonance condition for the wave number, produces the following equation for the growth rate

$$\gamma = \frac{2\pi\omega_p^2 v_{||}^2 \cos^2\left(\theta_{res}\right)}{\omega}\frac{\partial F}{\partial v_{||}}, \tag{6}$$

where θ_{res} is the resonance cone angle, which is determined by the values of the cyclotron and plasma frequencies [*Stix*, 1962; *Mosier and Gurnett*, 1969; *Gurnett and Bhattacharjee*, 2005].

The approach chosen to evaluate the growth rate was to perform an interpolation of the measured plasma distribution function, smooth it into a continuous mesh, and then approximate

the integration with a summation over the discrete points. Due to the close proximity that most of the data points have to each other, which limits the variation in the values of the distribution between points, a simple bilinear approximation method was utilized to create the smooth mesh. This smoothing took the roughly 300 ELS data points, which were oriented in a polar grid in velocity space, and transformed them into a linear grid containing well over 3000 points, making it easy to perform the necessary summations with good accuracy to obtain the reduced distribution function.

The first case we examine is the beam shown earlier, at or around 8:35 UT, in the region of burst-like low-frequency emission from Figure 26. Figure 28 displays the results of the analytical calculation of the growth rate at a representative frequency of f = 100 Hz for this time period. The values of the electron cyclotron and plasma frequencies listed earlier, $f_c \approx 10$ kHz and $f_p \approx 500$ Hz, were used in this calculation. The top panel is the reduced distribution function calculated from the bilinear interpolation and integration of the ELS data. The dashed region marks the photoelectrons generated by the spacecraft, which are not part of the Saturn environment but cannot be easily removed from the interpolated results. The beam appears after the photoelectrons, where an enhancement in the distribution forms a bump-on-tail distribution. The lower panel displays the calculated growth rates. Two significant regions of growth appear in the growth calculation, resulting from the two regions of positive slope in the distribution. This indicates that the beam, while dominated by 200 eV electrons, has multiple components. The resulting normalized growth rate, γ/ω, is very large, significantly greater than one. Such a large growth rate indicates a very rapidly growing instability, but violates the weak-growth approximation inherent in Kennel's equation, suggesting that another approach must be used to obtain an accurate growth rate in this case.

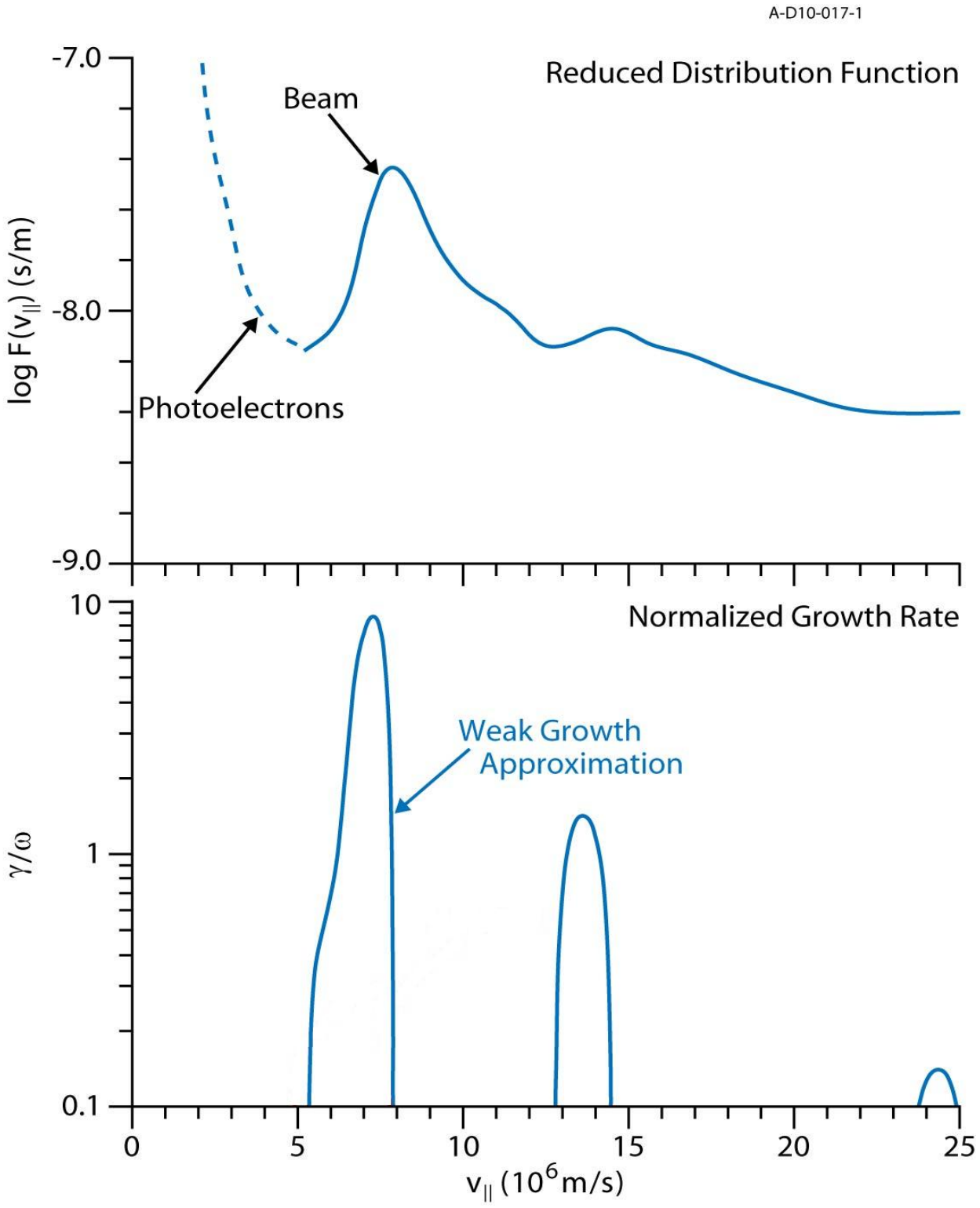

Figure 28 – Analytical growth rate results for the 8:35 UT beam on October 17, 2008. The powerful beam yields very large growth rates, indicating a breakdown in the weak growth approximation built into the analytical computation.

Time (UT)	Growth Rate	Beam Velocity (c)
7:07	0.0042	0.0205
7:11	0.0173	0.0525
7:45	0.3776	0.0840
7:48	0.1569	0.0777
7:51	0.2738	0.0240
8:19	0.3627	0.0354
8:29	0.3581	0.0189
8:32	1.2200	0.0221
8:35	6.8568	0.0240
8:39	1.3137	0.0259

Figure 29 – A table of results from the analytical calculations performed on ELS data from the October 17, 2008 event. The normalized growth rates and beam velocities are given for each time period that yielded a region of growth. Absent times produced no whistler-mode growth. Results from the periods 7:45-7:48 UT likely contain some additional error, as relativistic effects were not taken into account, but may be relevant at these velocities.

The 8:35 UT beam is not the only such event during this orbit. In analyzing all three-minute intervals from 7:00-9:00 UT, nine other intervals were found to contain beams at similar energies, though with the partial exception of the two time periods immediately flanking the 8:35 UT beam, all of these beams were considerably weaker in intensity. Analysis of these events using Equation (6) yielded growth rates over a wide range of values, from $\gamma/\omega \approx 0.004$ to 0.378 for those away from the 8:35 UT beam, all of which were deemed to be small enough that the weak growth approximation was valid. All of these beams coincided with regions of auroral hiss emission. A summary of these beams can be found in Figure 29.

5.3 Numerical Growth Rate Analysis

Since the analytical analysis did not yield accurate results for the beam observed at 8:35 UT, it is necessary to use some other technique that does not rely on the weak-growth approximation. Among the techniques that can be used is a computer program known as

WHAMP (Waves in Homogeneous Anisotropic Multicomponent Plasmas), which was developed by *Rönnmark* [1982; 1983] and designed to solve the dispersion relation for waves in a magnetized plasma for which the distribution function can be described as a sum of Maxwellian velocity distributions. The program allows for up to six distinct Maxwellian components, and yields a solution to the dispersion relation, as well as values for the growth rate and group velocity. The code yields a complete solution to the dispersion relation, without any further approximation.

In the case of the 8:35 UT beam, after subtracting out the spacecraft photoelectrons, two bi-Maxwellian components were used to fit the distribution, in order to provide dimension in both the parallel and perpendicular directions with respect to the magnetic field. These two components were fit to the two bumps in the distribution, which are shown in the top panel of Figure 27 at roughly 7 x 10^6 m/s and 14 x 10^6 m/s. In both cases, some of the input parameters, such as the density and temperature, could be determined from the RPWS and ELS instruments, while the other input parameters were adjusted to provide a good fit to the ELS measurement. This procedure was little more than a "guess-and-check" style method, adjusting each of the free parameters one by one until a good fit to the data was achieved. The result of this fitting is shown in the top panel of Figure 30, where two Maxwellian functions fit the two bumps of the distribution function. These Maxwellians were then inserted into the WHAMP calculation to determine a growth rate numerically, without relying on the weak-growth approximation.

In addition to the analytical results from Figure 28, the lower panel of Figure 30 also displays the numerical growth rates from the WHAMP calculation. These growth rates are significantly smaller than the analytical results, since WHAMP provides a full solution to the dispersion relation without assuming weak growth. However, the growth rates are still quite

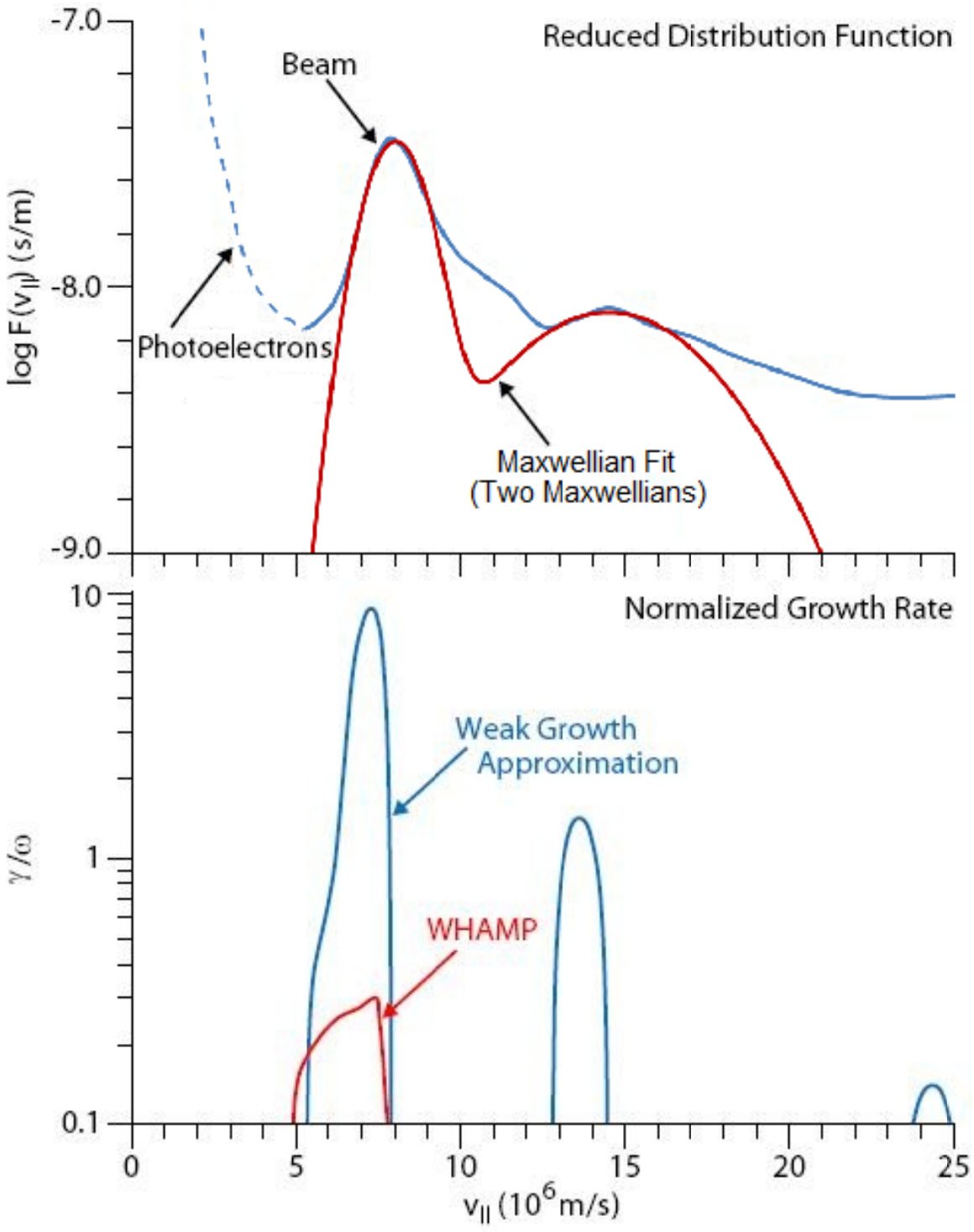

Figure 30 – A modified version of Figure 28, which now includes the numerical calculation results for the growth rates due to the 8:35 UT beam in addition to the analytical findings. The top panel shows the Maxwellian fits used to compute the growth rate using WHAMP, while the bottom panel shows this numerical result. The output of WHAMP, not relying on the weak growth approximation, produces a physical, but still very large, result for the growth rate.

large, $\gamma/\omega \approx 0.3$ for the first peak, and roughly 0.03 for the second peak (which is not shown, as it is too small to appear on the displayed scale), confirming that this beam is capable of producing the observed auroral hiss, as suggested by the analytical result. In fact, since the wave energy after a time t is proportional to $e^{2\gamma t}$, the growth of the wave energy associated with the stronger peak over just one second would be approximately e^{377} for a characteristic frequency of 100 Hz, large enough to be significant for even the smallest conceivable background intensities in the amplifying region.

5.4 Growth Rate Discussion

The previous section presented the analysis of a series of electron beams detected during the Cassini spacecraft's high-latitude pass on 17 October 2008. In each case, not only did the detected beam coincide with auroral hiss emission, but growth rate analyses demonstrated that each beam possessed large whistler-mode growth rates, sufficient to produce the observed emission intensities. In the case of the 8:35 UT beam, these growth rates were even so large as to violate the weak growth approximation.

Compared to auroral hiss typically observed at Earth, the emission observed during the period analyzed possesses two notable characteristics. First, instead of possessing a smooth upper boundary, the emission around 8:35 UT contains burst-like temporal variations on the order of the instrument's temporal resolution. These bursts appear in Figure 26 as fine structure at the higher frequencies of the auroral hiss emission. We considered the possibility that this pattern could be indicative of solitary wave structures, but inspection of the waveforms has not revealed the presence of any such waves. Analysis of high-resolution ELS data has revealed extremely large fluctuations in the beam intensity on time scales on the order of the ELS

instrument resolution, two seconds. With this in mind, it is not surprising to see short term temporal variations in the intensity of the auroral hiss, as variations in the beam intensity would produce variable growth rates. Furthermore, this region may contain emission due to ion conics, as reported by *Mitchell et al.* [2009], which are commonly observed at Saturn, and may enhance the wave intensity observed by the RPWS electric and magnetic sensors.

The other notable aspect of the emission is the occasional extension to frequencies above the local electron plasma frequency. Many of these extensions are observed around the time of the 8:35 UT beam. Since the whistler mode is restricted to frequencies below the lesser of the electron cyclotron frequency and electron plasma frequency, such an upward extension is not possible. However, because whistler-mode waves are driven into resonance as they approach the $f=f_p$ surface, the wave vector, k, becomes very large. At resonance, the corresponding wavelength becomes very small, and Doppler effects caused by spacecraft and plasma motions can become significant. These effects can push the observed emission in the spacecraft frame to higher frequencies than are present in the plasma rest frame, which would explain why the observed frequency occasionally extends above the plasma frequency.

The 8:35 UT beam on Day 291, 2008, was the first electron beam detected by CAPS at these energies. In the hope of discovering additional events to analyze, eight other orbits were selected for an intensive study, based on their similar qualities to Orbit 89 in terms of altitudes and L-shells surveyed during the orbits, as well as the prevalence of auroral hiss emissions. Although all of the high-latitude orbits have been studied, these eight were looked at in great detail, using very high resolution ELS data, to try to locate any sort of common detection. These eight orbits included the two flanking orbits, 88 and 90, as well as 72, 74, 78, 83, 86, and 93, all of which were not unlike the one orbit that had revealed this powerful beam. Despite this

extensive search, Orbit 89 still remains the only orbit to contain electron beam events like those evaluated in this chapter, as all eight of these additional orbits revealed no detections.

The reason for the lack of detections is unclear, although it is likely related to the strength and structure of the beams, as well as the propagation of these beams in relation to the auroral hiss emission. High-resolution ELS data of the beam events, as noted previously, has shown that these beams have dramatic variations in intensity on very short time scales, on the order of a few seconds. These large changes indicate that the beams generating the auroral hiss emission are likely very powerful, but very short in duration and narrow in structure. As a result, these beams may be difficult to detect if Cassini does not fly through the right region of space at the right time. Furthermore, as these beams and the auroral hiss propagate, there is no reason to believe that they will follow identical paths at an identical rate. On top of this, it is plausible that these very fine electron beams will be diffused in the magnetospheric environment at a considerably faster rate than the broader auroral hiss plasma wave. These discrepancies would make it possible, if not probable, to observe the auroral hiss emission without seeing its electron source.

Perhaps the most likely explanation for the absence of electron beam observations, however, involves the electron densities observed in the auroral regions during these high-latitude passes. Once outside the region of high density at low L-shells, the cold background plasma density drops considerably. In the case of the Day 291 event, the density drops considerably in a four-hour window from 6:00-10:00 UT, falling by three orders of magnitude from about 4 cm^{-3} to 4 x 10^{-3} cm^{-3}. These very low densities challenge the sensitivity of the CAPS instrument, making observations of electron beams highly unlikely.

One final concern that is worth addressing is the significant discrepancy between the analytical and WHAMP results for the 8:35 UT beam. Although the weak growth approximation

is obviously known to be at fault for at least part of the difference, the two results are separated by more than an order of magnitude, calling into questions whether the analytical method has an additional flaw in its application. To check this, a weaker beam was chosen, specifically the beam for 7:11 UT, which produced an analytical growth rate of roughly 0.017 when normalized to the real frequency. This growth rate shows no violation of the weak growth approximation, so the WHAMP approach should produce a similar result. Indeed, WHAMP yielded a normalized growth rate of about 0.015, verifying the analytical result in this case and implying that this method is still useful for providing accurate growth rates for weaker beams.

CHAPTER 6

SUMMARY

The study of auroral hiss is certainly not a new field in the study of space physics. As detailed in Chapter 2, a large collection of literature exists that covers roughly 50 years of analysis of this emission. However, most all of this had been done at Earth to this point. While this plethora of research has been important in gaining a better understanding of our planet and how this emission is produced, it is far from a conclusive answer to the processes that govern auroral hiss universally. As space physicists and astronomers often note, each planet in our solar system is unique, with each possessing its own quirks from the general norms. As such, it was crucial that a complete investigation of this emission be undertaken elsewhere in the solar system. The success of the Cassini mission has allowed for the first comprehensive study of Saturn and its local system, including this radio emission and its associated elements.

Chapters 1 and 2 detailed the fundamentals of our understanding of auroral hiss emission and how it is generated, with each experiment building on the previous ones. The early findings of good correlation between the observations of auroral hiss, electrons, and magnetic spectral density laid the foundation for the theory that was developed and expanded over the next decade. It became apparent that this process was part of a larger magnetospheric system, connected to the interaction of the solar wind with Earth that caused the visible aurora. The presumed generation by moving electrons led to several theories about how this emission was produced, but it took the idea of a coherent plasma instability to finally be able to explain the intensity of the emission that was being observed. Experiments such as those carried by sounding rockets and the space shuttle would confirm this theory, and the higher resolution of recent and current instrumentation has only increased our understanding of this phenomenon.

The Cassini spacecraft, carrying with it the instrumentation described in Chapter 3, provided the first opportunity to explore this emission and the theories behind it at a different planet in our solar system. The Saturn environment is considerably different than at Earth, and these variations would test the fundamentals that the theories of auroral hiss had been built on at Earth. At ten times the distance from the Sun, this gas giant planet experiences a far different impact from the solar wind, leaving open the possibility that it may not be the driving force in many of its magnetospheric and auroral emissions.

Since the latter half of 2006, Cassini has undergone two periods of high-latitude orbits of Saturn, totaling roughly 27 months of observations of the auroral regions. As detailed in Chapter 4, the early findings from the first series of these passes were far from surprising, and largely reflected the observations that had been made at Earth over the previous several decades. This emission was only observed when extending to the high-latitude regions where it was produced, but was detected frequently once Cassini was in those regions. The auroral hiss radio emission displayed the characteristic signatures of auroral hiss at Earth, most notably its funnel-shaped emission. Only a ledge-like step in the cutoff frequency on the low-latitude side of the emission deviated from the standard theories, but even this wasn't entirely surprising, as this feature had also been occasionally observed on Dynamics Explorer spectrograms at Earth.

However, the frequent observation of this ledge-like feature would prove to be crucial in the study of the larger system at Saturn. It was soon realized that this feature consistently lined up with a dramatic change in the electron density, and a series of field-aligned current structures consistently appeared in the same region. With all this in mind, it became apparent that this feature of auroral hiss had been an indicator of the presence of a higher density plasmasphere at lower latitudes, or more appropriately, lower L-shells. The plasmapause-like boundary of this

region, where the observed field-aligned currents reside, marks the beginning of the auroral zone, along with the ability to observe its emissions, including auroral hiss.

Perhaps an even more striking deviation from terrestrial auroral hiss has emerged from the study of the auroral hiss periodicity at Saturn. Instead of behaving in a clock-like manner, similar to its counterpart at Earth, Kronian auroral hiss acts as a rotating beam, a lighthouse-like beacon that co-rotates presumably with either the magnetospheric plasma or the planet itself. Furthermore, not only was this periodicity rotational, but the modulation rate was determined to be different in the two hemispheres, with the northern hemisphere rotating faster than the southern hemisphere. This coincided with previous studies of Saturn Kilometric Radiation (SKR), which also possessed the same hemispheric periodicity. Given the structure of the currents that would likely meet in the equatorial region, this dual periodicity is difficult to explain, as no unifying boundary condition exists at the equator for the two hemispheres.

When an electron beam was detected by the CAPS instrument during Orbit 89, the opportunity emerged to study the foundations of the generation of the auroral hiss radio emission that was being observed. As detailed in Chapter 5, attempts to calculate the whistler-mode growth rate of this beam analytically proved to be a successful failure, in that they showed remarkably large amounts of wave growth, but in doing so violated one of the assumptions inherent in the calculation, namely the weak-growth approximation. A numerical method, WHAMP, would later provide a more reasonable result for the growth, though even its result was very large. A few weaker beams at nearby times were also studied in the same orbit, yielding considerably smaller yet still significant results. Unfortunately, the lack of detections of any electron beams in any other orbits, most likely due to the very low densities in the auroral regions, prevented any further study of this kind.

All of these results are important in comparing Saturn's properties to those of Earth, but the findings of this study are not restricted solely to these two planets. The great amount of information gained by this research could also play a significant role in future space missions. One likely candidate is Juno, a planned spacecraft mission to Jupiter which will be able to detect and study auroral hiss there for the first time. This assumes of course that similar emissions exist at Jupiter, though observations of strong auroras and powerful Jovian Decametric Radiation suggest that auroral hiss is likely present as well. Juno is scheduled to launch in August 2011, and will enter into a polar orbit around Jupiter on October 19, 2016. Although much is known already about Jupiter's magnetosphere from previous spacecraft missions, Juno is certain to expand on this knowledge with its pioneering in situ measurements of the Jovian polar regions.

REFERENCES

Carlson, C.W., et al. (1998), FAST observations in the downward auroral current region: Energetic upgoing electron beams, parallel potential drops, and ion heating, *Geophys. Res. Lett*., *25(12),* 2017.

Cattell, C., et al. (2002), FAST observations of discrete electrostatic waves in association with down-going ion beams in the auroral zone, *J. Geophys. Res., 107(A9),* 1238, doi:10.1029/2001JA000254.

Cartwright, D.G., and P.J. Kellogg (1974), Observations of radiation from an electron beam artificially injected into the ionosphere, *J. Geophys. Res., 79*(10), 1439-1457.

Desch, M. D., and M. L. Kaiser (1981), Voyager measurements of the rotation period of Saturn's magnetic field, Geophys. Res. Lett., 8, 253–256, doi:10.1029/GL008i003p00253.

Dougherty, M.K., et al. (2004), The Cassini magnetic field investigation, *Space Sci. Rev., 114*, 331.

Ellis, G.R.A. (1957), Low-frequency radio emission from aurorae, *J. Atmos. Terr. Phys*., *10*, 302.

Ergun, R.E. et al. (1998), FAST satellite observations of electric field structures in the auroral zone, *Geophys. Res. Lett., 25(12)*, doi:10.1029/98GL00635.

Ergun, R.E., et al. (2003), Fast auroral snapshot satellite observations of very low frequency saucers, *Physics of Plasmas*, *10(2),* doi:10.1063/1.1530160.

Farrell, W.M., D.A. Gurnett, and C.K. Goertz (1989), Coherent Cherenkov radiation from the Spacelab 2 electron beam, *J. Geophys. Res., 94*, 443.

Farrell, W.M., et al. (1993), An interpretation of the broadband VLF waves near the Io torus as observed by Ulysses, *J. Geophys. Res., 98*, 21,177-21,188.

Gurnett, D.A., and B.J. O'Brien (1964), High-latitude geophysical studies with satellite Injun 3, 5. Very low frequency electromagnetic radiation, *J. Geophys. Res.*, *69(1),* 65.

Gurnett, D.A. (1966), A satellite study of VLF hiss, *J. Geophys. Res., 71(23)*, 5599.

Gurnett, D.A., S.R. Mosier, and R.R. Anderson (1971), Color spectrograms of very-low-frequency Poynting flux data, *J. Geophys. Res.*, *76(13),* 3022.

Gurnett, D.A., and L.A. Frank (1972), VLF hiss and related plasma observations in the polar magnetosphere*, J. Geophys. Res.*, *77(1),* 172.

Gurnett, D.A., W.S. Kurth, and F.L. Scarf (1979), Auroral hiss observed near the Io plasma torus, *Nature, 280*, 767-770, doi:10.1038/280767a0.

Gurnett, D.A., S.D. Shawhan, and R.R. Shaw (1983), Auroral hiss, Z mode radiation, and auroral kilometric radiation in the polar magnetosphere: DE 1 observations, *J. Geophys. Res., 88(A1),* 329.

Gurnett, D.A., et al. (1986), Whistler-mode radiation from the Spacelab 2 electron beam, *Geophys. Res. Lett., 13*, 225.

Gurnett, D.A., and U.S. Inan (1988), Plasma wave observations with the Dynamics Explorer 1 spacecraft, *Rev. of Geophys.*, *26(2),* 285.

Gurnett, D.A., et al. (2004), The Cassini radio and plasma wave investigation, *Space Sci. Rev., 114*, 395.

Gurnett, D.A., et al. (2005), Radio and plasma wave observations at Saturn from Cassini's approach and first orbit, *Science, 307*, 1255-1259, doi:10.1126/science.1105356.

Gurnett, D.A., and A. Bhattacharjee (2005), *Introduction to Plasma Physics With Space and Laboratory Applications*, Cambridge University Press, Cambridge, UK.

Gurnett, D. A., A. Lecacheux, W. S. Kurth, A. M. Persoon, J. B. Groene, L. Lamy, P. Zarka, and J. F. Carbary (2009a), Discovery of a north–south asymmetry in Saturn's radio rotation period, Geophys. Res. Lett., 36, L16102, doi:10.1029/2009GL039621.

Gurnett, D.A., A.M. Persoon, J.B. Groene, A.J. Kopf, G.B. Hospodarsky, and W.S. Kurth (2009b), A north-south difference in the rotation rate of auroral hiss at Saturn: Comparison to Saturn's kilometric radio emission, *Geophys. Res. Lett.*, 36, L21108, doi:10.1029/2009GL040774.

Gurnett, D.A., A.M. Persoon, A.J. Kopf, W.S. Kurth, M.W. Morooka, J.-E. Wahlund, K.K. Khurana, M.K. Dougherty, D.G. Mitchell, S.M. Krimigis, and N. Krupp (2010), A plasmapause-like density boundary at high latitudes in Saturn's magnetosphere, *Geophys. Res. Lett.*, in press, doi:10.1029/2010GL044466.

James, H.G. (1976), VLF saucers, *J. Geophys. Res., 81*, 501-514, doi:10.1029/JA081i004p00501.

Jorgensen, T.S. (1968), Interpretation of auroral hiss measured on OGO-2 and at Byrd Station in terms of incoherent Cherenkov radiation, *J. Geophys. Res., 73*, 1055.

Kennel, C. (1966), Low-frequency whistler mode, *Phys. Fluids, 9*(11), 2190-2202.

Kennel, C.F. and H.V. Wong (1967), Resonant particle instabilities in a uniform magnetic field, *J. Plasma Physics, 1(1),* 75.

Klumpar, D.M., R.J. Strangeway, C.W. Carlson, J.P. McFadden, and M.A. Temerin (1999), Latitude and local time distribution of downward direction ion beams in the auroral ionosphere, *Eos Trans. AGU, 80(17)*, *Spring Meet. Suppl.,* Abstract SM32D-09.

Kopf, A.J., et al. (2010), Electron beams as the source of whistler-mode auroral hiss at Saturn, *Geophys. Res. Lett., 37,* L09102, doi:10.1029/2010GL042980.

Krimigis, S.M., et al. (2004), Magnetosphere Imaging Instrument (MIMI) on the Cassini mission to Saturn/Titan, *Space Sci. Rev., 114*, 233.

Kurth, W.S., and L.A. Frank (1990), Spacelab 2 Plasma Diagnostics Package, *J. Spacecraft, 27(1),* 70.

Kurth, W.S., T.F. Averkamp, D.A. Gurnett, J.B. Groene, and A. Lecacheux (2008), An update to a Saturnian longitude system based on kilometric radio emissions, *J. Geophys. Res., 113, A05222*, doi:10.1029/2007JA012861.

Laaspere, T., W.C. Johnson, and L.C. Semprebon (1971), Observations of auroral hiss, LHR noise, and other phenomena in the frequency range 20 Hz to 540 kHz on Ogo 6, *J. Geophys. Res., 76*, 4477.

Lin, C.S., J.L. Burch, S.D. Shawhan, and D.A. Gurnett (1984), Correlation of auroral hiss and upward electron beams near the polar cusp, *J. Geophys. Res., 89(A2),* 925.

Lonnqvist, H., M. André, L. Matson, A. Bahnsen, L.G. Blomberg and R.E. Erlandson (1993), Generation of VLF saucer emissions observed by the Viking satellite. *J. Geophys. Res., 98*, 13565-13574.

Maggs, J.E. (1976), Coherent generation of VLF hiss, *J. Geophys. Res., 80(10),* 1707.

Martin, L.H., R.A. Helliwell, and K.R. Marks (1960), Association between aurorae and very low-frequency hiss observed at Byrd Station, Antarctica, *Nature, 187(4739),* 751.

Matson, D.L., L.J. Spilker, and J.P. Lebreton (2002), The Cassini/Huygens mission to the Saturnian system, *Space Sci. Rev.*, *104*, 1.

McEwen, D.J., and R.E. Barrington (1967), Some characteristics of the lower hybrid resonance noise bands observed by the Alouette 1 satellite, *Can. J. Phys., 45*, 13.

Mitchell, D.G., et al. (2009), Ion conics and electron beams associated with auroral processes on Saturn, *J. Geophys. Res., 114*, A02212, doi:10.1029/2008JA013621.

Monson, S.J., P.J. Kellogg, and D.G. Cartwright (1976), Whistler mode plasma waves observed on Electron Echo 2, *J. Geophys. Res., 81*(13), 2193-2199.

Morgan, D.D., D.A. Gurnett, J.D. Menietti, J.D. Winningham, and J.L. Burch (1994), Landau damping of auroral hiss, *J. Geophys. Res., 99(A2),* 2471.

Mosier, S.R., and D.A. Gurnett (1969), VLF measurements of the Poynting flux along the geomagnetic field with the Injun 5 satellite, *J. Geophys. Res., 74(24),* 5675.

O'Brien, B.J., C.D. Laughlin, and D.A. Gurnett (1964), High-latitude geophysical studies with satellite Injun 3, 1. Description of the satellite, *J. Geophys. Res., 69(1),* 1.

Persoon, A.M., et al. (1988), Electron density depletions in the nightside auroral zone, *J. Geophys. Res., 93(A3),* 1871.

Pfaff, R., C. Carlson, J. Watzin, D. Everett, and T. Gruner (2001), An overview of the Fast Auroral SnapshoT (FAST) satellite, *Space Sci. Rev., 98*, 1.

Rönnmark, K. (1982), WHAMP: Waves in homogenous, anisotropic multicomponent plasma, *Kiruna Geophysical Institute Report 179.*

Rönnmark, K. (1983), Computation of the dielectric tensor of a Maxwellian plasma, *Plasma Phys., 25,* 699-701, doi:10.1088/0032-1028/25/6/007.

Santolik, O., and D.A. Gurnett (2002), Propagation of auroral hiss at high altitudes, *Geophys. Res. Lett., 29(10),* doi:10.1029/2001GL013666.

Smith, R.L. (1969), VLF observations of auroral beams as sources of a class of emission, *Nature*, *224*(5217), 351-352.

Southwood, D. J., and M. G. Kivelson (2007), Saturnian magnetospheric dynamics: Elucidation of a camshaft model, J. Geophys. Res., 112, A12222, doi:10.1029/2007JA012254.

Stix, T.H. (1962), *The Theory of Plasma Waves*, McGraw-Hill, New York.

Taylor, W.W.L, and S.D. Shawhan (1974), A test of incoherent Cherenkov radiation for VLF hiss and other magnetospheric emissions, *J. Geophys. Res., 79*, 105.

Wu, C. S., and L. C. Lee (1979), A theory of the terrestrial kilometric radiation, Astrophys. J., 230, 621– 626, doi:10.1086/157120.

Xin, L., D.A. Gurnett, and M.G. Kivelson (2006), Whistler mode auroral hiss emissions observed near Jupiter's moon Io, *J. Geophys. Res., 111*, doi:10.1029/2005JA011411.

Xin, L., D.A. Gurnett, O. Santolik, W.S. Kurth, and G.B. Hospodarsky (2006), Whistler-mode auroral hiss emissions observed near Saturn's B-ring, *J. Geophys. Res., 111*, doi:10.1029/2005JA011432.

Young, D.T., et al. (2004), Cassini Plasma Spectrometer Investigation, *Space Sci. Rev., 114*, 1-112.